Geophysical Journal International

Geophys. J. Int. (2010) **183,** 313–329 doi: 10.1111/j.1365-246X.2010.04720.x

Underplating of the Hawaiian Swell: evidence from teleseismic receiver functions

Garrett M. Leahy,[1] John A. Collins,[1] Cecily J. Wolfe,[2] Gabi Laske[3] and Sean C. Solomon[4]

[1] *Department of Geology and Geophysics, Woods Hole Oceanographic Institution, Woods Hole,* MA 02543, *USA. E-mail: garrett.leahy@gmail.com*
[2] *Hawaii Institute of Geophysics and Planetology, University of Hawaii, Manoa, Honolulu,* HI 96822, *USA*
[3] *Cecil H. and Ida M. Green Institute of Geophysics and Planetary Physics, Scripps Institution of Oceanography, University of California, San Diego, La Jolla,* CA 92093, *USA*
[4] *Department of Terrestrial Magnetism, Carnegie Institution of Washington, Washington,* DC 20015, *USA*

Accepted 2010 July 2. Received 2010 July 2; in original form 2009 June 12

SUMMARY

The Hawaiian Islands are the canonical example of an age-progressive island chain, formed by volcanism long thought to be fed from a hotspot source that is more or less fixed in the mantle. Geophysical data, however, have so far yielded contradictory evidence on subsurface structure. The substantial bathymetric swell is supportive of an anomalously hot upper mantle, yet seafloor heat flow in the region does not appear to be enhanced. The accumulation of magma beneath pre-existing crust (magmatic underplating) has been suggested to add chemical buoyancy to the swell, but to date the presence of underplating has been constrained only by local active-source experiments. In this study, teleseismic receiver functions derived from seismic events recorded during the PLUME project were analysed to obtain a regional map of crustal structure for the Hawaiian Swell. This method yields results that compare favourably with those from previous studies, but permits a much broader view than possible with active-source seismic experiments. Our results indicate that the crustal structure of the Hawaiian Islands is quite complicated and does not conform to the standard model of sills fed from a central source. We find that a shallow *P*-to-*s* conversion, previously hypothesized to result from the volcano-sediment interface, corresponds more closely to the boundary between subaerial and subaqueous extrusive material. Correlation between uplifted bathymetry at ocean-bottom-seismometer locations and presence of underplating suggests that much of the Hawaiian Swell is underplated, whereas a lack of underplating beneath the moat surrounding the island of Hawaii suggests that underplated crust outward of the moat has been fed from below by dykes through the lithosphere rather than by sills spreading from the island centre. Local differences in underplating may reflect focusing of magma-filled dykes in response to stress from volcanic loading. Finally, widespread underplating adds chemical buoyancy to the swell, reducing the amplitude of a mantle thermal anomaly needed to match bathymetry and supporting observations of normal heat flow.

Key words: Heat flow; Body waves; Hotspots; Crustal structure.

1 INTRODUCTION

The Hawaiian-Emperor chain of islands and seamounts is perhaps the most striking feature of Pacific Ocean bathymetry (Fig. 1). The volcanic centres are characterized by a consistent age progression from the present to 75 Ma (Duncan & Keller 2004), with a relatively stable source of volcanism currently located at or just southeast of the island of Hawaii. To first-order, the age progression of the islands correlates well with the motion of the Pacific Plate over an approximately stationary point in the underlying mantle. This pattern has led researchers to propose Hawaii as a canonical example of the surface expression of a mantle plume, a thermal upwelling from deep in the mantle (e.g. Morgan 1971; Sleep 1992; White & McKenzie 1995). This hypothesis is supported by geochemical analyses showing that Hawaiian basalts are distinct from mid-ocean ridge basalts on the basis of both isotopic (Hart *et al.* 1992) and trace-element chemistry (Hofmann 1997), suggesting the presence of a mantle component that is not sampled by the global mid-ocean ridge system.

A primary feature of intraplate volcanic chains is the presence of a regional bathymetric high, or swell (Crough 1983). The swell surrounding the Hawaiian-Emperor chain, first described by Dietz &

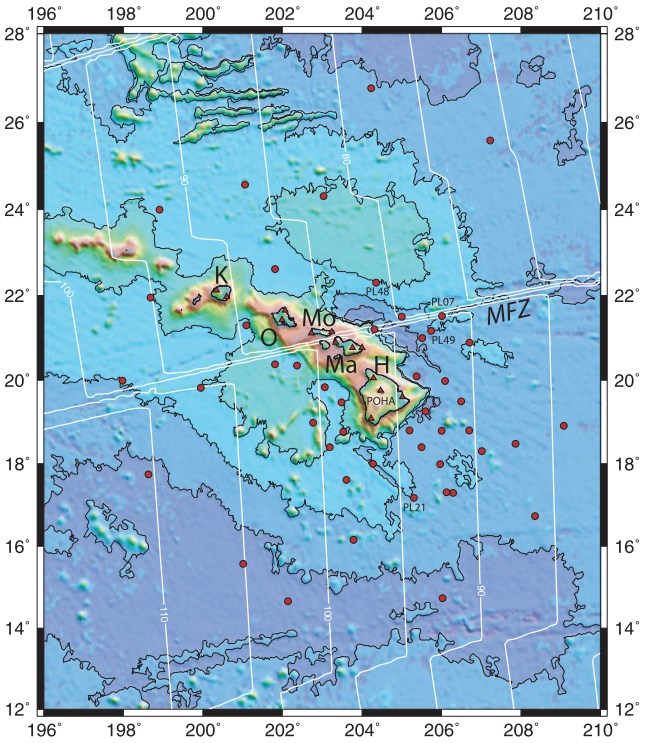

Figure 1. Bathymetry of the Hawaiian Swell (National Geophysical Data Center 2006). Contours are at 500-m intervals. Symbols denote the locations of instruments used in this study, with triangles representing land-based seismometers and circles representing OBSs. White lines depict approximate contours of crustal age (Müller *et al.* 2008). The Molokai Fracture Zone (MFZ) and major islands (H, Hawaii; Ma, Maui; Mo, Molokai; O, Oahu and K, Kauai) are labelled.

Menard (1953), is characterized by a maximum regional shoaling of the seafloor of approximately 1300 m (Fig. 1). Because lithospheric cooling models can account for the evolution of bathymetry and lithospheric structure in ocean basins (e.g. Parsons & Sclater 1977; Stein & Stein 1992; Zhong *et al.* 2007), swell regions are proposed to correspond to regions of anomalously hot (or reheated) lithosphere.

The classic model for the formation of hotspot swells relies on a positive buoyancy anomaly in the mantle as a response to thermal expansion (Crough 1978). Some models invoke 'thermal erosion' of the overlying lithosphere by a mantle plume (e.g. Detrick & Crough 1978; Sleep 1987, 1990, 1994), where heat from the plume conduit is conducted into the lower lithosphere and advected with the plate downstream from the plume location. Other models (e.g. Ribe & Christensen 1994) indicate that the swell can be supported by thermal buoyancy in the asthenosphere without lithospheric erosion.

Recent application of receiver function methods to the determination of the thickness of the seismic lithosphere in the region of Hawaii (Li *et al.* 2004) indicates substantial lithospheric thinning downstream from the active volcanoes and therefore favours the thermal erosion mechanism, while earlier measurements of Rayleigh wave group velocity along the island chain (Woods *et al.* 1991; Woods & Okal 1996; Priestley & Tilmann 1999) suggest negligible lithospheric thinning. Regional tomographic studies (e.g. Laske *et al.* 1999; Tilmann *et al.* 2001; Wolfe *et al.* 2002, 2009; Laske *et al.* 2007) and global studies (e.g. Montelli *et al.* 2004, 2006) have consistently imaged zones of low seismic velocity in the upper mantle beneath the Hawaiian Islands supporting both lithospheric and asthenospheric sources of thermal buoyancy. Though volatiles and melt may play roles in the reduction of seismic velocities, a seafloor magnetotelluric experiment (Constable & Heinson 2004) on the swell suggests that melt connectivity must be severely restricted to account for the highly resistive lithospheric lid.

Central to the hypothesis of thermal support of a hotspot swell is the corollary prediction that the seafloor heat flux should be enhanced at topographic highs (Crough 1978). However, extensive surveys of the Hawaiian Swell suggest that heat flow may be indistinguishable from values expected for the age of the surrounding seafloor (e.g. Von Herzen *et al.* 1989; Harris *et al.* 2000). The absence of a heat flow anomaly may pose an obstacle to a thermal origin for hotspot swells, suggesting either a small thermal anomaly or enhanced sublithospheric convection (Moore *et al.* 1998). Heat flow measurements on the Hawaiian Swell, however, may be considerably underestimated due to local hydrothermal circulation (Harris & McNutt 2007).

The subsidence history of the Hawaiian-Emperor island and seamount chain as recorded in coral reefs (e.g. Griggs 1997) has generally been thought to be consistent with the rapid cooling of a thermal anomaly in the shallow mantle. However, analyses of geoid height, seismic structure, and flexural response to volcanic loading have shown that the swell evolution is considerably more complex (e.g. Watts *et al.* 1985a; Brocher & ten Brink 1987; Watts & ten Brink 1989; Wessel 1993a,b; Verzhbitsky *et al.* 2006). Deviations from the standard cooling model have inspired researchers to interpret variations in geophysical observables in terms of temporal variations in the flux of melt through the system (e.g. Davies 1992; Vidal & Bonneville 2004; Van Ark & Lin 2004).

Robinson (1988) and Phipps Morgan *et al.* (1995) proposed that significant chemical buoyancy may be added beneath the lithosphere by melt extraction. This hypothesis helps to reconcile inconsistencies between the lack of a resolvable heat flow anomaly and the size of the swell by reducing the magnitude of the required lithospheric thermal anomaly. Phipps Morgan *et al.* (1995) further proposed that this signal may be complemented by buoyancy added to the base of the oceanic crust via magmatic underplating of the crust in the vicinity of the swell, which would also act to reduce the subsidence due to lithospheric cooling.

Here, we use the term magmatic underplating to refer to the process by which mantle-derived melts are trapped in the shallowest mantle below extant crust. Generally characterized as a network of sills and dykes radiating from a source of magma, underplating is manifested frequently in seismic data as 'anomalously slow' mantle, with observed seismic velocities intermediate between standard lower crust and uppermost mantle. Underplating is likely present to varying degrees in many regions with active surface volcanism; its presence has been well established beneath volcanic islands including Hawaii (e.g. Watts *et al.* 1985b; Wolfe *et al.* 1994; Caress *et al.* 1995; McNutt & Bonneville 2000; Leahy & Park 2005). This phenomenon differs from crustal intrusion (where magma penetrates extant crust), common beneath rifted continental margins (e.g. Holbrook & Kelemen 1993; Harland *et al.* 2009; White & Smith 2009). Previous estimates of the maximum crustal thickness beneath the Hawaiian Islands range from 15 to 20 km (Watts *et al.* 1985b; ten Brink & Brocher 1987; Li *et al.* 1992; Wölbern *et al.* 2006), compared with an average thickness of 6.2 km off the swell (Lindwall 1991).

In this study, we present a regional model of crustal structure derived from receiver function (RF) analysis of teleseismic *P* wave coda collected during the Hawaiian Plume–Lithosphere Undersea Melt Experiment (PLUME). The PLUME project consisted of

2-yr-long deployments of ocean-bottom seismometers (OBSs) and portable island-based stations. The ocean-bottom networks offer unprecedented coverage of the Hawaiian Swell, allowing a determination of the likely extent and thickness of underplating beneath and surrounding the islands. Although RF analysis of OBS data presents unique challenges in the form of low signal-to-noise ratios at short periods and a limited catalogue of events, we show that our method compares favourably to crustal structure derived from other seismic techniques where available, thereby increasing the confidence in our findings.

Our results indicate that shallow bathymetric anomalies correlate with the presence of crustal underplating, indicating that the Hawaiian Swell is partially supported by shallow chemical buoyancy. Further, we find that crustal thickness may vary rapidly from station to station. The depth of the Mohorovičić (Moho) discontinuity, or crust–mantle boundary, is approximately constant where underplating is present, even along the island chain. Finally, we find that the deepest portions of the Hawaiian flexural moat have no measurable underplating and therefore considerably thinner crust than adjacent regions. Our observations suggest that underplating at Hawaii does not conform to the standard model of hotspot structure.

2 DATA

In the Hawaiian PLUME study, national instrument pool sensors from Woods Hole Oceanographic Institution and Scripps Institution of Oceanography were deployed in two phases. First, a network of OBSs spaced ∼75 km apart and surrounding the island of Hawaii was deployed from 2005 January to 2006 January to provide high-resolution images of the upper mantle beneath the current centre of volcanism. Stations from the first deployment are numbered PL01 to PL35. The second deployment was a large-aperture outer network of OBSs spaced ∼250 km apart and operating from 2006 April to 2007 June, designed to provide deeper resolution and extend coverage across the swell. These stations are numbered PL36 to PL74. In conjunction with the OBS deployments, 10 portable broadband instruments from the Carnegie Institution of Washington's Department of Terrestrial Magnetism were deployed on the islands of Hawaii, Maui, Molokai, Oahu and Kauai.

We have augmented this data set by the inclusion of data from the Incorporated Research Institutions for Seismology (IRIS) Global Seismographic Network stations KIP on Oahu and POHA on Hawaii and GEOFON station MAUI on Maui, where improved site characteristics and greater data quantity help verify the quality of results from the short-term deployments. Prior to analysis, the horizontal OBS orientations were determined using teleseismic *P*-wave particle motions (Wolfe *et al.* 2009).

For each station, events were high-pass filtered above 0.1 Hz to remove long-wavelength variations in amplitude. Events were then evaluated visually on the basis of the following three characteristics: (1) clear visibility of a *P*-wave arrival, (2) signal-to-noise ratio (from inspection) greater than 2 and (3) positive polarity for the calculated RF at the *P*-wave arrival. These conditions, particularly the signal-to-noise condition, substantially reduced the number of events available at ocean stations, but they yield greater confidence in the imaged structure. Station location and number of events are listed in Table 1. In addition to the stringent data selection criteria, mechanical failure and unrecovered instruments (Laske *et al.* 2009) limited coverage for this study to 44 of the 74 originally deployed OBS stations, in addition to the 10 temporary and three permanent land stations.

3 METHOD

For this study, we compute multiple-taper cross-correlation RFs (Park & Levin 2000). This method involves frequency-domain deconvolution and adds frequency-dependent variance weighting to stacks of RF data, permitting greater confidence in imaged structure at higher frequencies. In addition, we compute bootstrap uncertainties at each station, in order to quickly determine which peaks in the RF are statistically robust (Leahy & Collins 2009; Park & Levin 2010).

Receiver functions ideally give two pieces of information: the amplitude of correlation between the radial and vertical components (related to the impedance contrast at an interface in the Earth), and the *Ps* delay time of the arrival (a function of the depth of a *P*-to-*s* wave conversion interface and the overlying seismic velocity structure). With a forward-model approach based on the predicted arrival times from crustal reverberations (Zhu & Kanamori 2000), Leahy & Park (2005) determined that layers in the crust at oceanic hotspots are too thin to constrain the ratio of the compressional wave speed to the shear wave speed, V_P/V_S. Instead, they used a fixed velocity model to show that travel times of direct and reverberated pulses that complicate oceanic island RFs can be matched by a three-layer model: a top layer of extruded volcanic material, a middle layer composed of normal crustal material formed at a mid-ocean ridge, and a lower layer formed by magmatic intrusions into the uppermost lithospheric mantle (Fig. 2). Nomenclature for direct arrivals and modelled reverberations follows the convention that with the exception of the first letter, capital letters refer to downgoing waves and lower-case letters refer to upgoing waves in a layer.

Ps delay times of reverberations and the direct arrival are calculated as functions of slowness p and velocity structure in a fashion similar to that of Zhu & Kanamori (2000)

$$\tau(p) = \sum_{j=1}^{n} \left[h_j B_j(p) - h_j A_j(p)\right] + \sum_s h_i B_i(p) + \sum_p h_i A_i(p), \quad (1)$$

where n is the deepest interface sampled by the reverberation, sums over s and p are over paths travelling through a homogeneous layer i as S or P waves, respectively, and

$$A_i(p) = \sqrt{\frac{1}{V_{p_i}^2} - p^2}; \qquad B_i(p) = \sqrt{\frac{1}{V_{s_i}^2} - p^2}, \quad (2)$$

where V_{p_i} and V_{s_i} denote the compressional and shear wave speeds of the ith layer, respectively. For example, the crustal reverberation $Pp_1P_1s_1$ travels upwards through layer 1 as a P wave, reflects off the surface, and converts to an upgoing S wave at the interface at the base of layer 1. The reverberation time is therefore:

$$\tau_{Pp_1P_1s_1}(p) = h_1 B_1(p) - h_1 A_1(p) + 2h_1 A_1(p) = h_1 B_1(p) + h_1 A_1(p). \quad (3)$$

Reverberations may sample multiple layers. For example, the reverberation $Ps_3s_2P_2P_3s_3s_2s_1$ is a version of the *PsPs* reverberation in underplated oceanic crust, sampled at an island station. The delay

Table 1. Station information.

Station	Events	Lat (°N)	Lon (°W)	Elev. (m)	Type	M	UP?	*V* (km)	OC (km)	*U* (km)	CT (km)	DTM (km)
BIG2	36	19.08	155.77	582	Land	H	√	2.3	5.0	4.1	12.2	11.6
BYUH	8	21.65	157.93	23	Land	H	√	3.8	6.7	6.2	17.9	17.9
CCHM	29	20.77	156.00	60	Land	H	√	2.9	3.9	11.3	19.1	19.0
DLAH	14	19.60	154.98	52	Land	H	√	3.5	9.2	7.4	21.2	21.1
HPAH	17	20.05	155.71	775	Land	H	√	2.6	6.1	6.7	16.3	15.5
KCCH	28	21.97	159.40	128	Land	H	√	2.6	4.9	7.0	15.4	15.3
KIP	30	21.42	158.02	70	Land	H	√	5.1	7.3	5.0	19.1	19.0
LHSM	27	20.89	156.66	204	Land	H	√	5.2	6.3	7.1	20.3	20.1
MAUI	17	20.77	156.00	60	Land	H	√	4.7	5.8	5.6	17.7	17.6
MRKH	14	21.11	157.27	143	Land	H	√	3.9	6.1	6.3	17.6	17.5
NGOK	13	22.12	159.66	1157	Land	H	√	4.8	6.1	8.7	21.2	20.0
PHRM	28	21.14	156.76	407	Land	H	√	3.5	6.0	7.0	17.7	17.3
POHA	244	19.76	155.53	1886.7	Land	H	√	3.9	4.8	9.0	19.0	17.1
PL01	16	20.09	154.62	−5580	OBS	H	√		6	8	14	20
PL03	14	21.21	155.68	−5144	OBS	L	√		4	7	11	16
PL05	3	21.51	154.99	−5196	OBS	L	×		6		6	11
PL06	16	21.00	154.48	−5393	OBS	L	×		6		6	11
PL07	13	21.52	153.98	−4912	OBS	L	√		7	8	15	20
PL08	12	20.89	153.29	−5157	OBS	H	√		8	8	16	21
PL10	10	19.98	153.90	−5336	OBS	L	×		7		7	12
PL11	11	19.50	153.50	−5181	OBS	H	×		6		6	11
PL13	10	19.26	154.39	−5515	OBS	L	√		6	6	12	18
PL14	15	18.80	153.99	−5252	OBS	L	√		6	4	10	15
PL15	11	18.80	153.30	−5077	OBS	L	×		6		6	11
PL17	10	18.48	152.13	−5184	OBS	L	×		6		6	11
PL20	10	17.30	153.70	−5120	OBS	L	×		8		8	13
PL21	14	17.18	154.69	−5010	OBS	L	×		6		6	11
PL22	14	17.99	154.03	−5057	OBS	L	×		6		6	11
PL23	12	18.40	154.50	−5167	OBS	L	×		6		6	11
PL24	14	18.80	154.80	−5319	OBS	H	×		6		6	11
PL27	13	18.00	155.72	−5099	OBS	L	×		5		5	10
PL29	16	18.40	156.81	−4627	OBS	L	×		7		7	12
PL31	10	18.77	156.47	−4610	OBS	L	×		7		7	12
PL32	16	18.98	157.23	−4605	OBS	H	√		5	7	12	16
PL33	12	19.48	156.51	−4707	OBS	H	√		6	8	14	19
PL34	12	19.83	156.93	−4748	OBS	L	√		6	7	13	18
PL35	13	20.35	157.63	−4650	OBS	L	√		8	9	17	22
PL36	12	21.30	158.90	−4762	OBS	L	√		9	8	17	21
PL37	13	19.82	160.05	−4676	OBS	L	×		7		7	12
PL38	4	19.99	162.03	−4897	OBS	L	×		7		7	12
PL39	11	21.96	161.31	−4543	OBS	H	√		7	9	16	21
PL40	17	24.00	161.09	−4701	OBS	H	√		6	4	10	14
PL41	11	24.57	158.93	−4749	OBS	L	×		6		6	10
PL43	11	26.78	155.77	−5545	OBS	L	×		6		6	11
PL44	6	25.59	152.77	−5420	OBS	L	×		7		7	12
PL46	6	24.31	156.96	−4428	OBS	L	×		7		7	11
PL47	12	22.62	158.19	−4828	OBS	L	√		7	8	15	19
PL48	11	22.30	155.64	−4528	OBS	H	√		6	4	10	14
PL49	9	21.17	154.25	−5175	OBS	H	×		6		6	11
PL55	2	18.30	152.98	−5076	OBS	L	×		8		8	13
PL57	6	18.91	150.91	−5335	OBS	L	×		7		7	12
PL61	3	16.74	151.64	−5186	OBS	L	×		7		7	12
PL63	8	14.73	153.97	−5607	OBS	L	×		9		9	14
PL65	8	17.32	153.87	−5115	OBS	L	×		7		7	12
PL66	8	17.61	156.39	−4826	OBS	L	×		8		8	13
PL67	8	16.16	156.21	−5116	OBS	L	×		9		9	14
PL68	8	14.66	157.86	−5637	OBS	L	×		6		6	11
PL70	10	15.57	158.98	−5590	OBS	L	×		6		6	12
PL71	10	17.75	161.37	−5601	OBS	L	×		6		6	11
PL74	9	20.38	158.18	−4541	OBS	L	√		5	6	11	16

Notes. Stations are listed by the number of events utilized for this study, location and station type. M denotes method (H, high frequency and L, low frequency). UP? where not √ s denotes underplating present. *V* denotes volcanic layer. OC denotes normal oceanic crust. *U* denotes the thickness of magmatic underplating. CT denotes total crustal thickness. DTM denotes depth to Moho (relative to sea level) inferred from this study. Where a decimal place is given, typical uncertainties average ±0.2 km; elsewhere we estimate uncertainties of ±0.5 km.

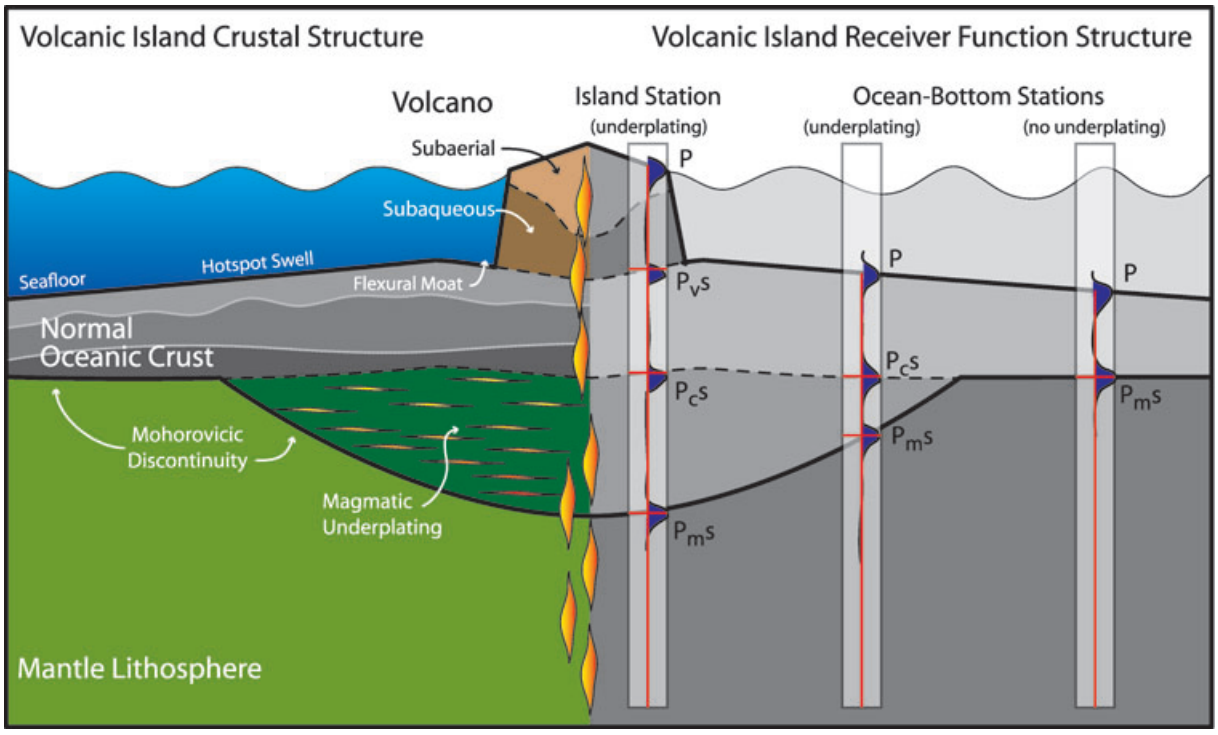

Figure 2. Schematic of crustal structure at an oceanic hotspot. The left side shows the standard model of oceanic crust near a volcano, while the right shows a schematic of *P*-to-*s* conversions from interfaces (neglecting reverberations). Normal oceanic crust is sandwiched between extruded volcanic material (both subaqueous and subaerial) and a region of magmatic intrusions at the top of the lithospheric mantle, termed magmatic underplating. The Moho conversion (P_ms) provides a measure of the depth extent of this modification. In regions where underplating is present, a conversion is seen from the base of the normal crust (P_cs) as a mid-crustal interface. Stations located on extruded volcanic material also see a shallow conversion (P_vs) from a volcanic interface.

time for this phase is

$$\tau_{Ps_3s_2P_2P_3s_3s_2s_1} = \sum_{j=1}^{3}[h_jB_j(p) - h_jA_j(p)] + 2(h_3B_3(p) + h_2B_2(p)) + h_3A_3(p) + h_2A_1(p). \quad (4)$$

A complete list of phases modelled in this study is presented in Table 2. It should be emphasized that ocean-bottom instruments are generally at the top of the second layer; the volcanic layer is utilized only at land stations. Because not all interfaces are present beneath all stations, we will refer in the text to a *P*-to-*s* conversion at the base of the deepest crustal layer as P_ms (the 'true' Moho), one at the interface between magmatic underplating and normal oceanic crust where present as P_cs, and one at the base of shallow volcanic material as P_vs.

Analysis of RF data in this data set has confirmed the poor constraints that reverberations place on V_P/V_S ratio for thinly layered structure. Further, the amplitude of a *Ps* conversion can be strongly affected by event signal-to-noise ratio and local variability in interface structure. We find that whereas RFs calculated from synthetic seismograms can provide visual confirmation of structure inferred from actual earthquake data, we cannot determine interface impedance contrast with confidence.

We therefore use a fixed velocity model (Table 3) and solve for layer thicknesses that best explain the timing and polarities of the direct arrival and a train of later-arriving reverberated phases, as in Leahy & Park (2005). This model has been modified to reflect current estimates of seismic velocities in the extruded volcanic layer (Eccles *et al.* 2009). There is a trade-off between velocity structure and layer thickness, and certainly we expect variations in velocity structure over the study region (e.g. Lindwall 1988; Park *et al.* 2007). However, we find that our RF estimates of interface depth agree well with those from local refraction surveys where available (see Section 4), and therefore we are confident extending this velocity model to the entire region with the understanding

Table 2. Primary and reverberated phases modelled in this study.

Phase	Polarity	
Layer 1		
Ps_1	+	Primary
$Pp_1P_1s_1$	+	
$Ps_1P_1s_1$	−	Equivalent to $Pp_1S_1s_1$
Layer 2		
Ps_2s_1	+	Primary
$Pp_2P_2s_2s_1$	+	
$Ps_2P_2s_2s_1$	−	
$Pp_2p_1P_1P_2s_2s_1$	+	
$Ps_2s_1P_1P_2s_2s_1$	−	
Layer 3		
$Ps_3s_2s_1$	+	Primary
$Pp_3P_3s_3s_2s_1$	+	
$Ps_3P_3s_3s_2s_1$	−	
$Pp_3p_2P_2P_3s_3s_2s_1$	+	
$Ps_3s_2P_2P_3s_3s_2s_1$	−	
$Pp_3p_2p_1P_1P_2P_3s_3s_2s_1$	+	
$Ps_3s_2s_1P_1P_2P_3s_3s_2s_1$	−	

Notes. Some legs on reverberated paths are interchangeable without changing the arrival time or the polarity, particularly *PsPs* and *PpSs* and similar paths.

Table 3. Velocity model.

Layer	V_P (km s^{-1})	V_S (km s^{-1})
Volcanic material	4.90	2.60
Normal oceanic crust	6.30	3.60
Underplated material	7.30	4.2
Mantle	8.16	4.75

Notes. The trade-off between layer thickness and seismic velocities in thin crustal layers does not permit an accurate determination of the local velocity structure using a phase stacking method. We therefore use a three-layered crustal model (Leahy & Park 2005) that gives results similar to refraction studies.

that small perturbations to the model will slightly influence layer thicknesses.

The need for corrections to the reference model is evident in some of the synthetic RFs shown in Section 4, where some conversion arrival times, particularly multiples, arrive before (or after) those in the data. We subsequently show that the model we have chosen explains first-order structure where external constraints (a refraction survey) exists, suggesting that it is sufficient as an average regional model.

Each layer thickness is determined by choosing the thickness that corresponds to the maximum value of stacked amplitude. We can estimate uncertainty via Taylor expansion, relating the curvature at the best-fitting layer thickness to the standard deviation of the stacked amplitude (Zhu & Kanamori 2000, eq. 6). For stations where we applied this method, the uncertainty in layer thickness averages ± 0.2 km. Because the standard deviation is related to the number of reliable events in the stack, uncertainties are smaller at stations with more usable earthquakes. The uncertainty is frequency dependent because frequency influences the curvature at the best-fitting layer thickness; we have analysed all land stations at 2.0 Hz for consistency.

During our analysis, we found the maximum reliable cut-off frequency for the RF calculation to be site dependent. Generally, island stations were considered robust up to 2 Hz, while the permanent stations were reliable to frequencies in excess of 3 Hz. OBS RFs, while suffering from high levels of microseismic noise, also saturate from coherence in the water-column and sediment-layer reverberations. The maximum accessible frequency before saturation ranged from 0.5 to 1.5 Hz.

At low frequency (below 1 Hz), it is impossible to determine the precise arrival time for a primary conversion from the first crustal layer because the conversion is obscured by the direct *P* arrival. We avoided this difficulty by instead measuring the arrival time of the crustal reverberation (e.g. $Pp_1P_1s_1$), which we can then use to calculate layer thickness. Later-arriving pulses (signalling underplating) have a distinct character that can easily be distinguished from single-interface crustal structure. Careful consideration of synthetic RFs and predicted reverberation times suggests that our estimates using this method can tolerate ± 0.5 km uncertainties in layer thickness without markedly influencing the character of the RF.

4 RESULTS

We determined the thickness of crustal layers beneath each station in the PLUME network and have summarized the results in Table 1. For each station, we show the location, number of events used in the calculations, whether or not underplating is present (UP?), whether the high (H) or low (L) frequency method (M) was used, and the thicknesses in kilometres of the volcanic layer (V), normal oceanic crust (OC) and magmatic underplating (U), as well as the total crustal thickness (CT) and the depth to the Moho discontinuity (DTM) relative to sea level. A detailed station map and the complete suite of observed RFs are presented in the Supporting Information (online). In Figs 4–9, we give examples of the observed RFs and calculated synthetic RFs to demonstrate interpretation. For the RF figures shown in the paper, we use overlapping epicentral distance bins that are 10° wide and centred every 5° to display the data for optimal clarity. In the Supporting Information the bins are 5° wide and centred every 2.5°. At many stations, variation in the delay time of P_ms with backazimuth implies the presence of a dipping or non-uniform interface, but this pattern is ignored in favour of first-order structure to simplify comparisons among stations. Finally, it should be noted that the OBS stations in this experiment are not located on extruded volcanic material, and therefore we do not expect to see (or model) a P_vs conversion from the base of the volcano.

RFs (at 2 Hz cut-off frequency) are plotted versus epicentral distance at POHA, the permanent GSN station on Hawaii, in Fig. 3. Primary conversions P_vs, P_cs and P_ms are clear in the stacks, as are many reverberations (not identified for clarity). The results of Leahy & Park (2005) are confirmed with the much larger data set presented here. The structure seen at POHA is representative of the RFs at all island stations, with varying degrees of clarity.

Examples of RFs from OBSs where we have determined that underplating is present are shown in Figs 4–7. For sites PL01 and PL48 (Figs 4 and 5, respectively), primary conversions P_cs and P_ms are clearly visible, as well as the full crustal reverberation *PpPs*. At stations PL07 and PL74 (Figs 6 and 7), in contrast, we are not able to access sufficiently high frequencies to make a direct determination of crustal thickness. We can therefore consider the arrival of the full-crustal reverberation and the character of the RF trace to determine the thickness of crustal layers. We find that underplating is required to fit the reverberations.

Examples of ocean-bottom seismic stations where underplating is not indicated are shown in Figs 8–11. Stations PL11 and PL49 have sufficient data quality and quantity to calculate high-frequency RF estimates (Figs 8 and 9, respectively). A primary conversion (P_ms) is evident, as well as prominent reverberations, but there is no evidence supporting the presence of underplating. At stations PL06 and PL21 (Figs 10 and 11, respectively) we are not able to recover sufficiently high frequencies to make a direct determination of crustal thickness. Consideration of the arrival time of the reverberated *PpPs* phase allows estimation of crustal thickness, and no underplating is required at these locations.

A summary of the results of this study is shown in map view in Fig. 12, including areas where underplating is required, areas where underplating is not indicated, and areas where the extent of underplating is poorly constrained. Several first-order features are evident. First and foremost, the area of underplating appears to coincide with the bathymetric swell. Second, the deepest 'moat' feature surrounding Hawaii is characterized by a clear lack of magmatic underplating. These characteristics are discussed further in Section 5.

Maps of the thickness of individual layers in the idealized crustal column are shown in Fig. 13. For each figure the contours and shading correspond to a tension surface fit through measurements at each station (triangles are land stations, circles are ocean-bottom stations). The areas shown should therefore be interpreted only as estimates (particularly in regions far from any station).

The map of the thickness of the normal oceanic crustal layer (Fig. 13a) shows that this layer is of relatively constant thickness

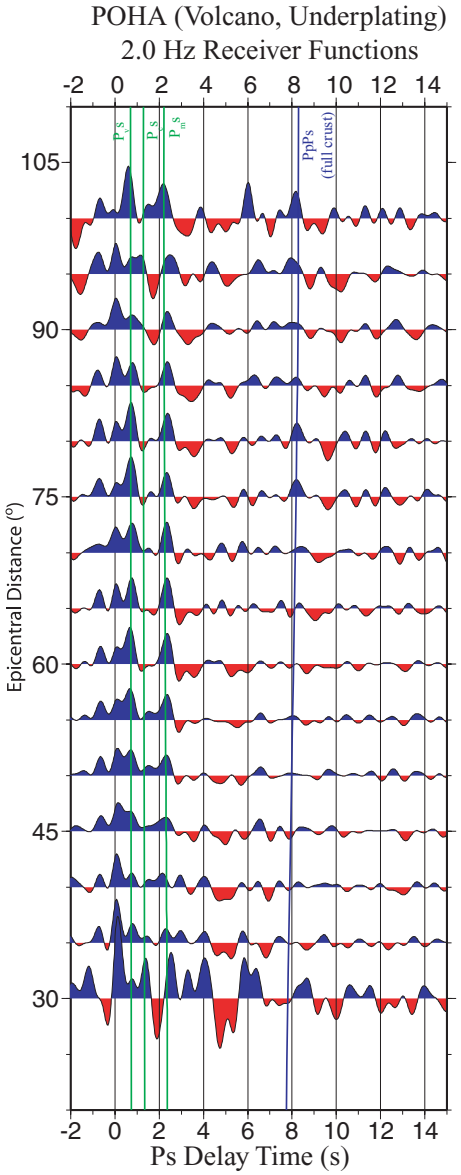

Figure 3. Receiver functions at GSN station POHA plotted versus epicentral distance (2-Hz cut-off frequency). Primary conversions P_vs, P_cs and P_ms are clear in the stacks (green lines), as are many reverberations (for example, *PpPs*, blue line). The crustal structure indicated by this RF is representative of that seen at all island stations considered in this study: a layer of extruded volcanic material, a middle layer of normal oceanic crust, and a lower most layer of magmatic underplating (see Fig. 2).

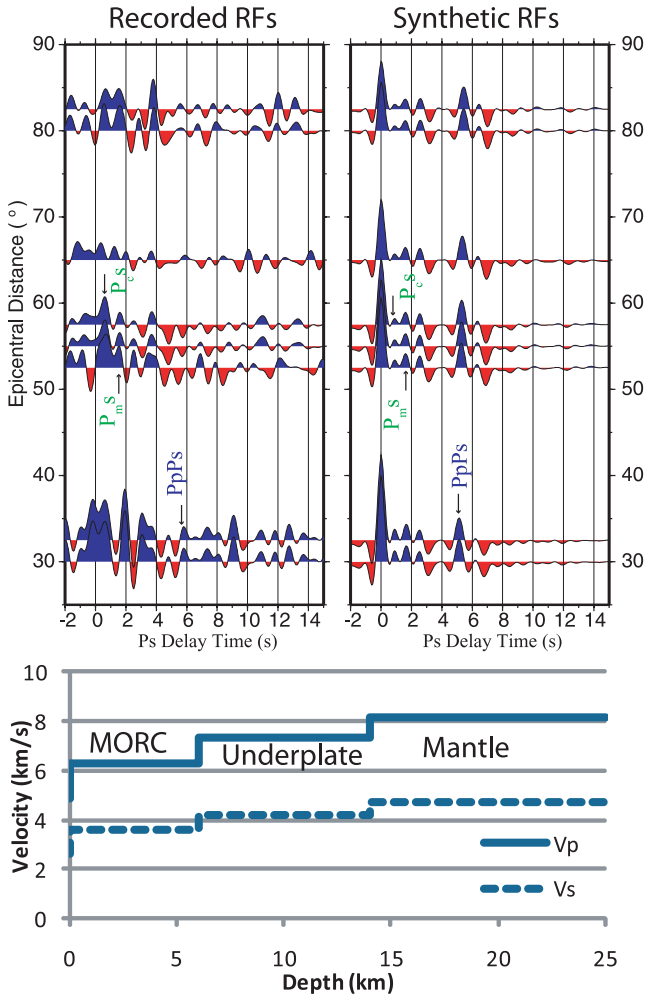

Figure 4. Observed receiver functions from station PL01 plotted versus epicentral distance (left-hand panel). Primary conversions are clearly identified (P_cs and P_ms), as are reverberations. Synthetics (right-hand panel) reproduce first-order characteristics of the data for a two-layered model with underplating (bottom panel).

and is not strongly affected by the presence of surface volcanism. This result indicates that the prior oceanic crust in this area had a relatively uniform response to both loading from above and melt flux from below. The average inferred thickness is 6.5 ± 1 km.

The thickness of the underplated layer (Fig. 13b), where observed, shows underplating to be of greatest extent under the volcanic islands, as would be expected if formed by a related process. The inferred thickness of the underplated layer ranges between 3.5 and 11.3 km, with an average thickness of 7.0 ± 2 km in areas where this layer is indicated by the observations.

The total thickness of the crustal column is shown in map view in Fig. 13(c). Not surprisingly, the variation has a large contribution from extrusive volcanic material on the islands. A lower than typical crustal thickness is apparent north of Hawaii, a topic that will be discussed further in Section 5. Total crustal thickness over the entire region ranges from 5 to 20 km, with an average thickness of 17 ± 2 km beneath the islands and 7 ± 1 km in non-underplated oceanic regions.

We also show the depth below sea level of the base of the crust in Fig. 13(d). This map corrects for the variations in station elevations, particularly between land and seafloor stations, and therefore depicts more clearly variations in interface depth among stations. This figure shows that the Moho depth is relatively constant throughout the underplated region, averaging 17 ± 3 km below sea level.

In order to compare cross-sections of crustal structure in different parts of the Hawaiian Swell, we have divided the chain into five distinct sections (Fig. 14). In panels (b)–(f), we plot crustal structure for each section as a function of distance from the 'hotspot axis,' which for simplicity is taken as a line connecting the permanent seismic stations POHA and KIP. Because these cross-sections represent 3-D models collapsed to a single line of section, variability in interface depth indicated by symbol locations may be as much indicative of large-scale 3-D structure as local variability.

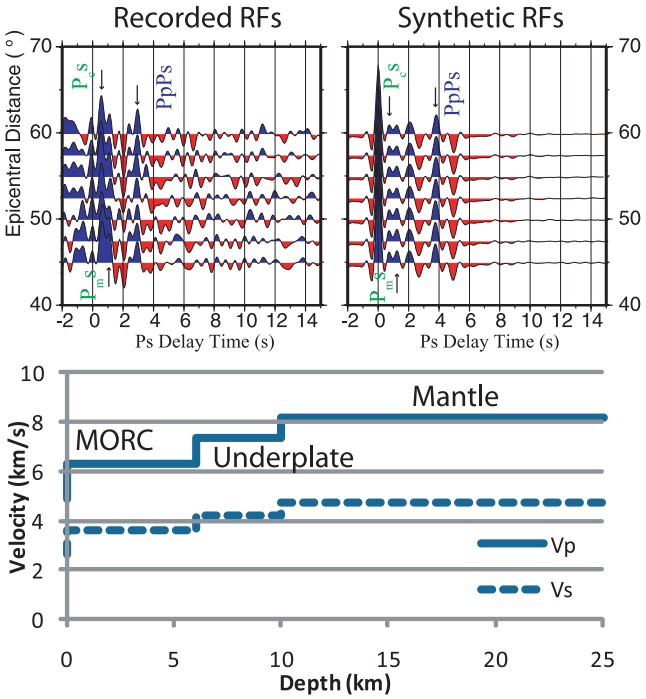

Figure 5. Observed receiver functions from station PL48 plotted versus epicentral distance (left-hand panel). Primary conversions are clearly identified (P_cs and P_ms), as are reverberations. Synthetics (right-hand panel) reproduce first-order characteristics of the data for a two-layered model with underplating (bottom panel).

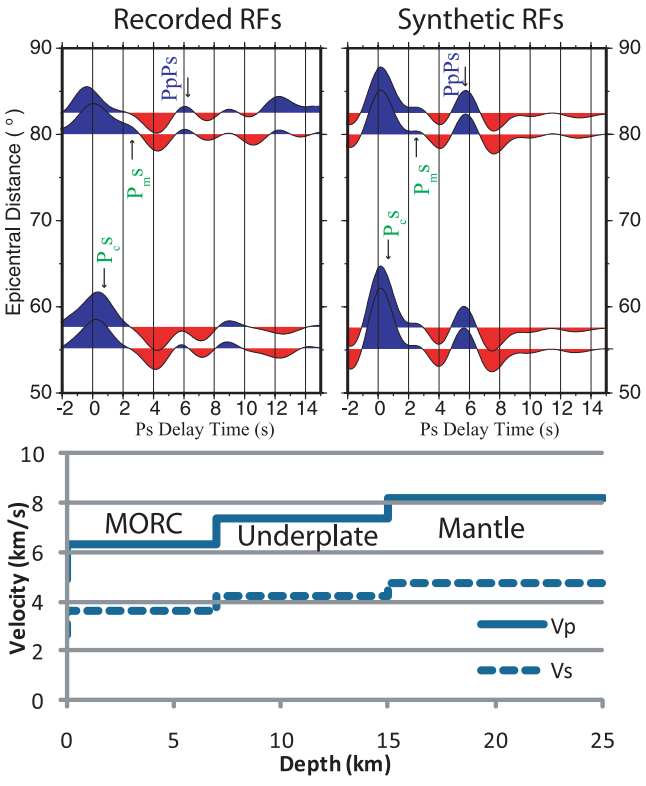

Figure 6. Observed receiver functions from station PL07 plotted versus epicentral distance (left-hand panel). Reverberations are identified. Synthetics (right-hand panel) reproduce first-order characteristics of the data from a two-layered model with underplating (bottom panel).

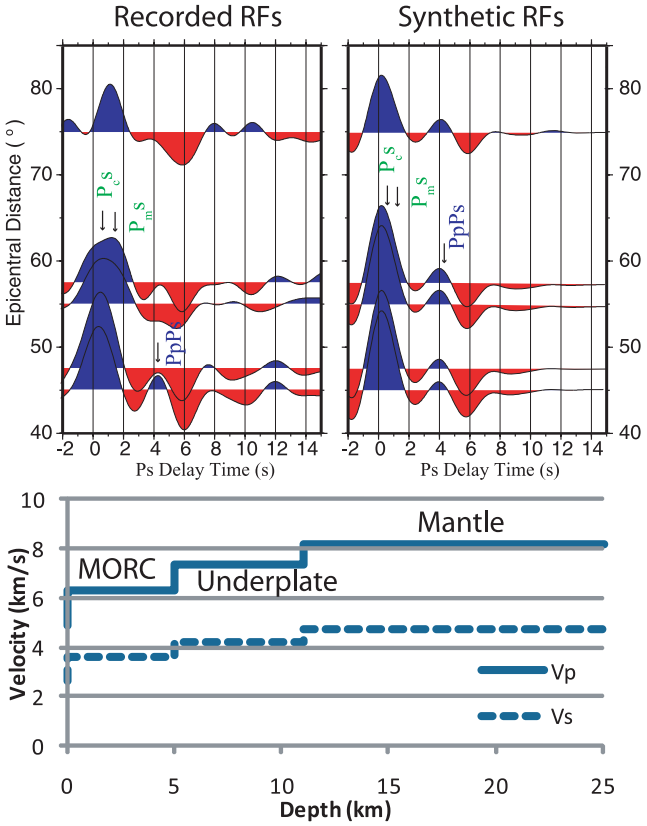

Figure 7. Observed receiver functions from station PL74 plotted versus epicentral distance (left-hand panel). Reverberations are identified. Synthetics (right-hand panel) reproduce first-order characteristics of the data from a two-layered model with underplating (bottom panel).

An 'Upwind' section is shown in Fig. 14(b). From Fig. 12 this section is seen to be mostly crust that has not been modified by the hotspot. Indeed, relatively uniform structure is recovered.

A section spanning Hawaii is shown in Fig. 14(c). Underplating is clearly seen to reach a maximum beneath the island, but closer examination shows a break in underplating at ±150 km from the axis, outside of which underplating is again indicated but in lesser amounts. Further, there is substantial variability in the depth of the P_cs conversion, though beneath the island that depth is correlated with the P_vs conversion, preserving the total thickness of the normal oceanic crustal layer. That the P_vs conversion beneath the islands is frequently found above the depth to nearby seafloor indicates that this interface may not mark the base of the extrusive layer, but perhaps rather the interface between subaerially and subaqueously extruded basalts.

The Maui/Molokai section (Fig. 14d) shares many features with the Hawaii section, including the presence of a local thinning of the underplated layer approximately 200 km from the islands. The Kauai section (Fig. 14e) also shows underplating, but there is insufficient station coverage to resolve any local thinning in the underplated layer.

To benchmark our results, we compare the results of our RF analysis to those from the expanding spread profiles of Watts *et al.* (1985b) in the Oahu section (Fig. 14f). This comparison tests both our method for determining interface depth and the accuracy of the velocity model we use in this study. We find that interface depths obtained via our RF method (symbols) compare favourably with major reflectors from the Watts *et al.* (1985b) study (lines).

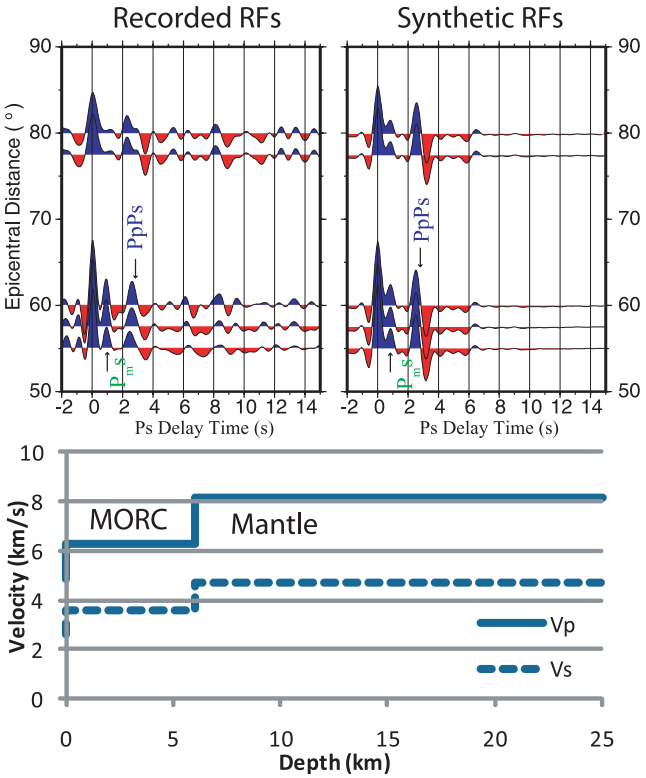

Figure 8. Observed receiver functions from station PL11 plotted versus epicentral distance (left-hand panel). A primary conversion is clearly identified (P_ms), as are reverberations. Synthetics (right-hand panel) reproduce first-order characteristics of the data with a single crustal layer (bottom panel).

The magnitude and lateral extent of underplating appear to agree, though our spatial resolution is limited by low station density.

5 DISCUSSION

5.1 Source of conversions

This study was undertaken with the assumption of a simple 'standard model' of crustal structure in mind: an extruded volcanic layer (marked at its base by the P_vs phase), a middle layer of normal oceanic crust (P_cs), and a deep layer of magmatic underplating (P_ms). To first-order, this model is consistent with the results of this study, particularly in that underplating is found in the vicinity of all of the Hawaiian Islands.

This model may be too simple for several reasons, however, particularly directly beneath the islands. First, the P_vs conversion in Fig. 14(f) is located at shallow depths and appears to correspond more closely to the interface between subaqueously and subaerially extruded volcanic material than the top of the normal oceanic crustal layer. If this interpretation holds, we would expect to see a correlation between station elevation (a proxy for the combined effects of loading and subsidence) and the thickness of this layer, but land stations in this study do not span a sufficient range of elevations to clearly define any trends. This interpretation is at variance with the premise that the P_vs phase is the result of the presence of the strong impedance contrast imparted by a thin sediment layer at the base of the volcano (Leahy & Park 2005). This mismatch between expected and observed conversion depths is not likely to be an artefact of our velocity model. To push the P_vs conversion deeper by 2 km would require a 10 per cent higher shear velocity, which does not seem reasonable for porous (and perhaps fluid rich) extruded basalt. The seismic velocities of the deeper crustal layers would also have to be simultaneously reduced to maintain similarity to the results from seismic refraction experiments.

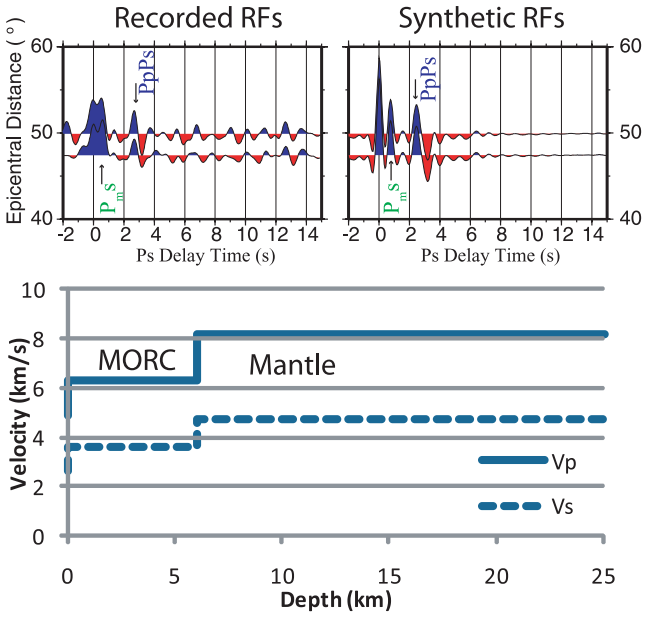

Figure 9. Observed receiver functions from station PL49 plotted versus epicentral distance (left-hand panel). A primary conversion is clearly identified (P_ms), as are reverberations. Synthetics (right-hand panel) reproduce first-order characteristics of the data with a single crustal layer (bottom panel).

For comparison, the shallowest pillow basalts in the Hawaiian Scientific Drilling Project (HSDP) cores are found at 2 km depth (DePaolo *et al.* 1999). Although slightly shallower than we measure, decreased seismic velocities of hyaloclastites above 3 km could account for the difference. We consider our seismic results to be generally consistent with the HSDP cores.

Further, if the P_vs conversion is not the interface between the volcanic material and normal oceanic crust a question is raised regarding the interpretation of the P_cs conversion. In subsidence and flexure models (e.g. Watts *et al.* 1985b; Brocher & ten Brink 1987; Wessel 1993a), the oceanic crust is deflected by several kilometres by volcanic loading, creating sharply dipping reflectors. This geometry has been confirmed by refraction studies in the vicinity of the islands. Our study, on the other hand, finds a surprisingly uniform depth to the P_cs conversion along the chain: 10.5 ± 2 km, in spite of what is presumed to be heterogeneous structure beneath each island. Dipping layers can influence both the amplitude and the timing of RF conversions and require substantial coverage in back azimuth to accurately resolve, so our interface depths may not be well constrained.

Perhaps the conversions we have resolved occurred at a mix of the top and bottom of normal oceanic crust, as one or the other might preferentially scatter energy beneath different stations. It is also remarkable that this layer remains uniformly thick, especially beneath the islands, where the P_vs conversion is found to lie above the depth of nearby seafloor. Considered on its own, this result would imply no deflection of the oceanic crust.

The most robust interpretation of a conversion interface is the base of magmatic underplating, which thickens under islands and correlates well with results from refraction studies. The timing of

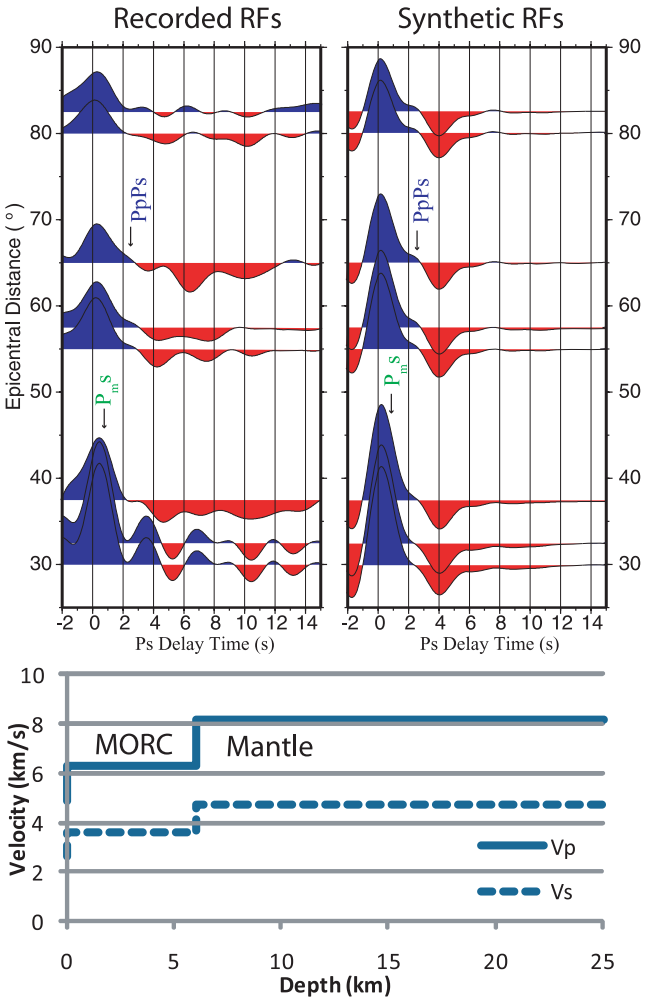

Figure 10. Observed receiver functions from station PL06 plotted versus epicentral distance (left-hand panel). Primary conversions are not clearly identified, but a reverberated phase is present. Synthetics (right-hand panel) reproduce first-order characteristics of the data with a single crustal layer (bottom panel).

the converted phase from this interface and the full reverberations confirm seismic velocities that are intermediate between crustal and mantle velocities.

5.2 Origin of underplating

Because many of our observations of crustal thickness do not include any evidence for underplating, it is clear that we are observing a process that is related to the formation of the Hawaiian Islands. The presence of underplating (Fig. 12) therefore relates to the complex process of magma transport through older (∼80–105 Ma) oceanic lithosphere. At a midplate hotspot such as Hawaii, magma-filled cracks sampling sublithospheric melts are thought to propagate through the lithosphere to the surface (e.g. Lister & Kerr 1991; Rubin 1995).

Flow in the mantle that results in partial melting, whether through decompression melting at sites of upwelling or chemically induced solidus reduction (via volatiles or fertile components), occurs over broad regions (Schubert *et al.* 2001). Because melts appear to be discretely sampled at the surface at both volcanic centres and mid-ocean ridges, most studies of melt migration have focused on the

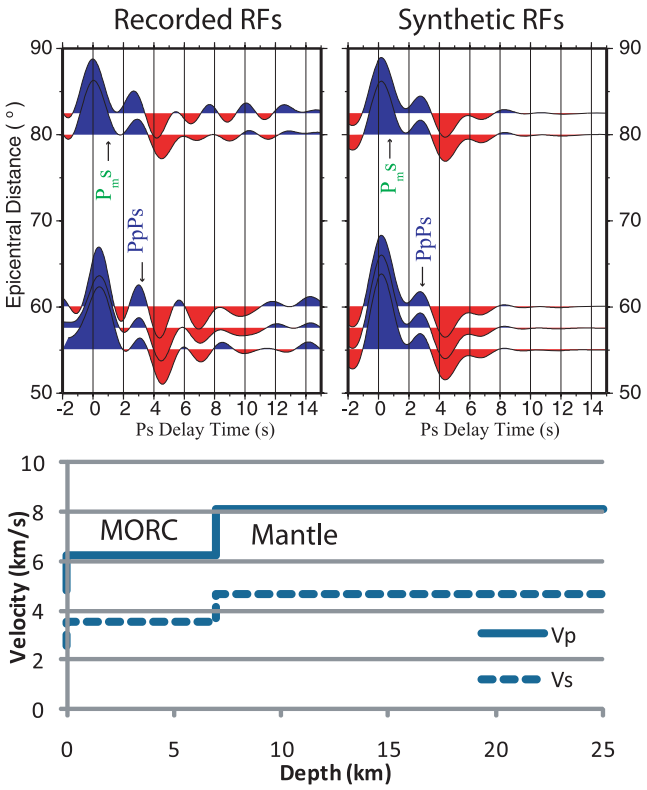

Figure 11. Observed receiver functions from station PL21 plotted versus epicentral distance (left-hand panel). Primary conversions are not clearly identified, but a reverberated phase is present. Synthetics (right-hand panel) reproduce first-order characteristics of the data with a single crustal layer (bottom panel).

question of how melts originating in a broad source region focus to localized and compositionally isolated channels (e.g. McKenzie 1984; Sparks & Parmentier 1991; Spiegelman 1993; Kelemen *et al.* 1997).

Specifically in the context of volcanic island chains, ten Brink (1991) found that the spacing between volcanoes was related to the elastic thickness of the oceanic lithosphere. His result suggests that the stress state of the lithosphere resulting from volcanic loading determines the ability for magma-filled dykes to propagate to the surface. Moreover, the growth of a volcano and flexure of the lithosphere may eventually shut off melt transport close to the load, leading to the nucleation of a new island (Hieronymus & Bercovici 1999, 2001).

Previous studies of underplating at ocean islands have suggested that seismic velocities intermediate between those of the lower crust and uppermost mantle are best explained by gabbroic sills propagating laterally away from a centralized source of melt (e.g. Wolfe *et al.* 1994; Caress *et al.* 1995), similar to some models for the formation of lower crust at ridges (e.g. Korenaga & Kelemen 1997). The correspondence between the structure obtained in this study and that of Watts *et al.* (1985b) support this hypothesis to some extent. In particular, we confirm that underplating extends beyond the edge of extrusive volcanism.

However, we also find that underplating extends at least 250 km from the islands (station PL07), and further that underplating at the leading edge of the hotspot is highly localized. This pattern indicates that a model of melt provided by a focused conduit is oversimplified, and underplated melts may in fact be derived from a broader region of the upper mantle. The gap in underplating northeast of the island

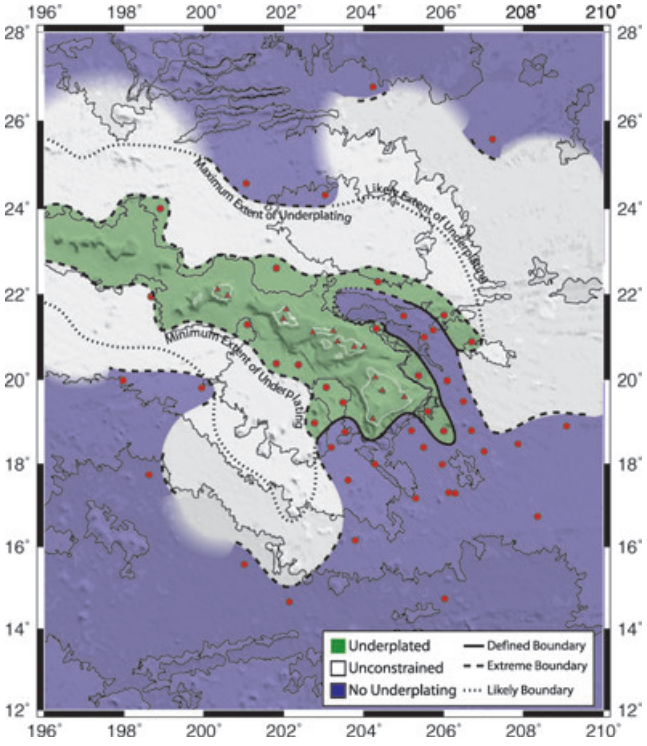

Figure 12. Map of magmatic underplating. Underplating is confirmed in the green region, and no underplating is indicated in the blue region. Low station density in the grey area leaves underplating unconstrained, so that underplating could perhaps extend anywhere between the minimum and maximum limits shown (dashed lines). A best estimate inferred from data in this study as well as the shape of the Hawaiian Swell is given by the dotted line.

of Hawaii, in particular, suggests that the system in the outermost area of underplating is fed from below rather than from the current locus of volcanism.

On the basis of laboratory analogues and numerical models, Muller *et al.* (2001) suggested the possibility of a feedback between volcanic loading and melt focusing, by which larger volcanoes focus dyke propagation towards their centres and therefore draw melt from a larger region of the lithosphere. The lack of underplating in the moat surrounding Hawaii (and to a lesser extent Maui) may lend support to this model, in that melt may have been preferentially focused towards the island. However, the absence of an underplating gap at the older Hawaiian Islands of Oahu and Kauai suggests either a minimum volcano size or unique perturbation to the local stress state. This pattern may be related to the passage of the Molokai Fracture Zone over the asthenospheric melt source, because fracture zones have been shown to influence local crustal structure (ten Brink & Brocher 1988; Wessel 1993b).

The scenario of Muller *et al.* (2001) may also explain the lack of small seamounts evident in bathymetry (Fig. 1) close to the Hawaiian Islands, and their resurgence on the Hawaiian Arch, because nearby melt is focused to the primary volcanoes. That other island chains in the Pacific (for example the Societies or Cook-Australs) are smaller and more dispersed perpendicular to the inferred age progression further supports the hypothesis that an initial disturbance in stress or volcanic load is necessary to create highly linear chains (Hieronymus & Bercovici 2000). Station coverage in this study is not sufficient to explore quantitatively any underplating in the vicinity of Hawaiian Arch seamounts, but a detailed study is possible with the methods described here.

Some researchers have suggested that melting may be initiated by decompression in the flexural arch (Bianco *et al.* 2005), and that this melting may be responsible for late-stage post-erosional alkalic volcanism on the islands and offshore (for example, the North Arch Volcanic Province, Clague *et al.* 1990). Our observations of underplating surrounding the island of Hawaii suggest that if decompression melting occurs beneath the arch, it happens without a time lag, in contrast with the several million years of lag observed with posterosional volcanism (Clague 1987). However, the present study cannot establish the causality of underplating in the flexural arch: chemical buoyancy may have enhanced deformation, or the underplating may have enhanced flexure.

Regarding the crustal structure of the islands themselves, we find several notable trends. First, while total crustal thickness does vary from station to station, Fig. 15 shows that the average depth to Moho is relatively constant at 17 ± 3 km. This is an intriguing observation, considering that the volcanic flux has been postulated to have varied strongly in time (Davies 1992; Van Ark & Lin 2004; Vidal & Bonneville 2004).

Our measurements provide strong evidence that underplating reflects the physical state of the system rather than the melt flux. We hypothesize that the greatest depth of underplating may reflect a level of neutral buoyancy for low-degree mantle-derived melts, which accumulate in magmatic sills. While we do not have the lateral resolution in this study to determine the interface gradient (how the lateral extent of underplating varies with depth), that information would be crucial in understanding how the intrusive process works both here and at other volcanic islands.

It is also possible to compare our inferred crustal structure against geochemical trends. The thickness of the underplated layer is shown as a function of distance along the island chain in Fig. 16. Station locations have been identified as belonging either to the Kea (triangles) or Loa (circles) volcanic trends (after Ihinger 1995). While our station coverage does not adequately sample the Loa trend, the data suggest that distinct chemical trends (for example, in lead isotopes, Abouchami *et al.* 2005) may correlate with a difference in thickness of underplating. Both the chemical trends and the difference in underplating thickness vanish near Oahu. If the thickness of the underplated layer is related to melt properties as opposed to flux, comparing these trends in the future may shed light on whether the chemical trends are caused by preferential melting of different mantle components. Notably, neither the volcanic layer nor the normal oceanic crustal layer display identifiable differences between volcanic trends.

5.3 A compositional origin for the Hawaiian Swell

The regional nature of the measurements obtained in this study allows us to investigate several possible avenues for causes of underplating. First and foremost, we find that underplating is present on both sides of the hotspot axis and that there is no correlation between crustal thickness and crustal age. From this result we infer that underplating is directly related to the Hawaiian volcanism and no other secondary feature. A plot of the crustal thickness obtained in this study versus ocean-bottom station bathymetry is shown in Fig. 17. Stations displaying underplating tend to be on average 275 m shallower than stations without underplating. This observation leads us to hypothesize that a component of the Hawaiian Swell may be chemically supported, similar to the chemical support of the Marquesas Swell proposed by Wolfe *et al.* (1994) and McNutt & Bonneville (2000).

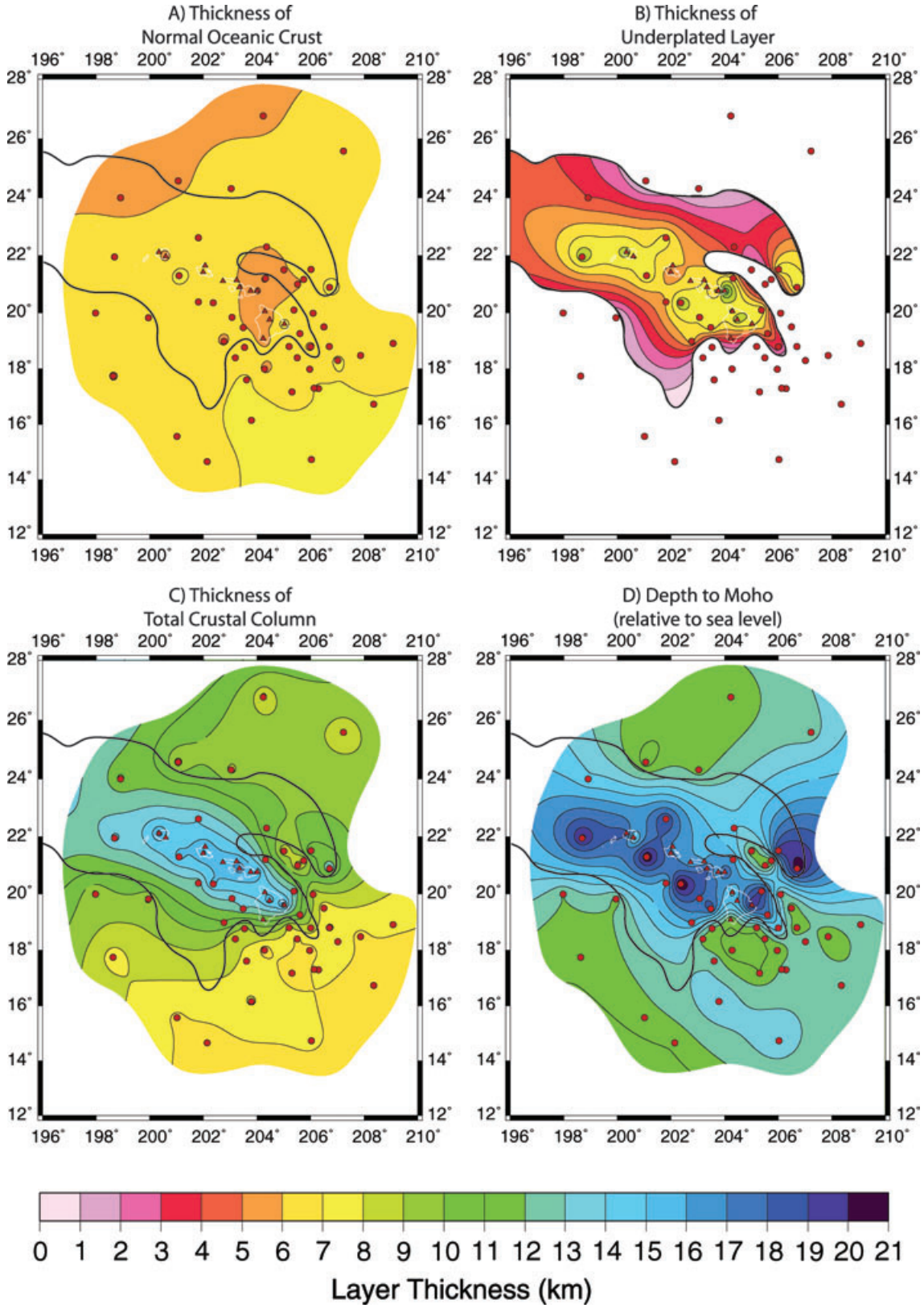

Figure 13. Maps of crustal layer thicknesses in the study region. Land stations are marked by triangles, and ocean-bottom stations by circles. Shading and contours (thin black lines) are at 1-km intervals. The likely extent of underplating (see Fig. 12) is shown as a thick black line. Unconstrained regions of the tension surface fit to observations are masked. (a) Thickness of the normal oceanic crust is relatively constant throughout the study region, averaging 6.5 ± 1 km. (b) Thickness of the underplated layer, masked for likely extent. This layer averages 7.0 ± 2 km in thickness. (c) Thickness of the total crustal column ranges from approximately 7 ± 1 km in non-underplated areas to 17 ± 2 km under the islands; the extruded volcanic material makes up a substantial fraction of this thickness. (d) Depth (from sea level) to the base of the crust averages 17 ± 3 km under the islands.

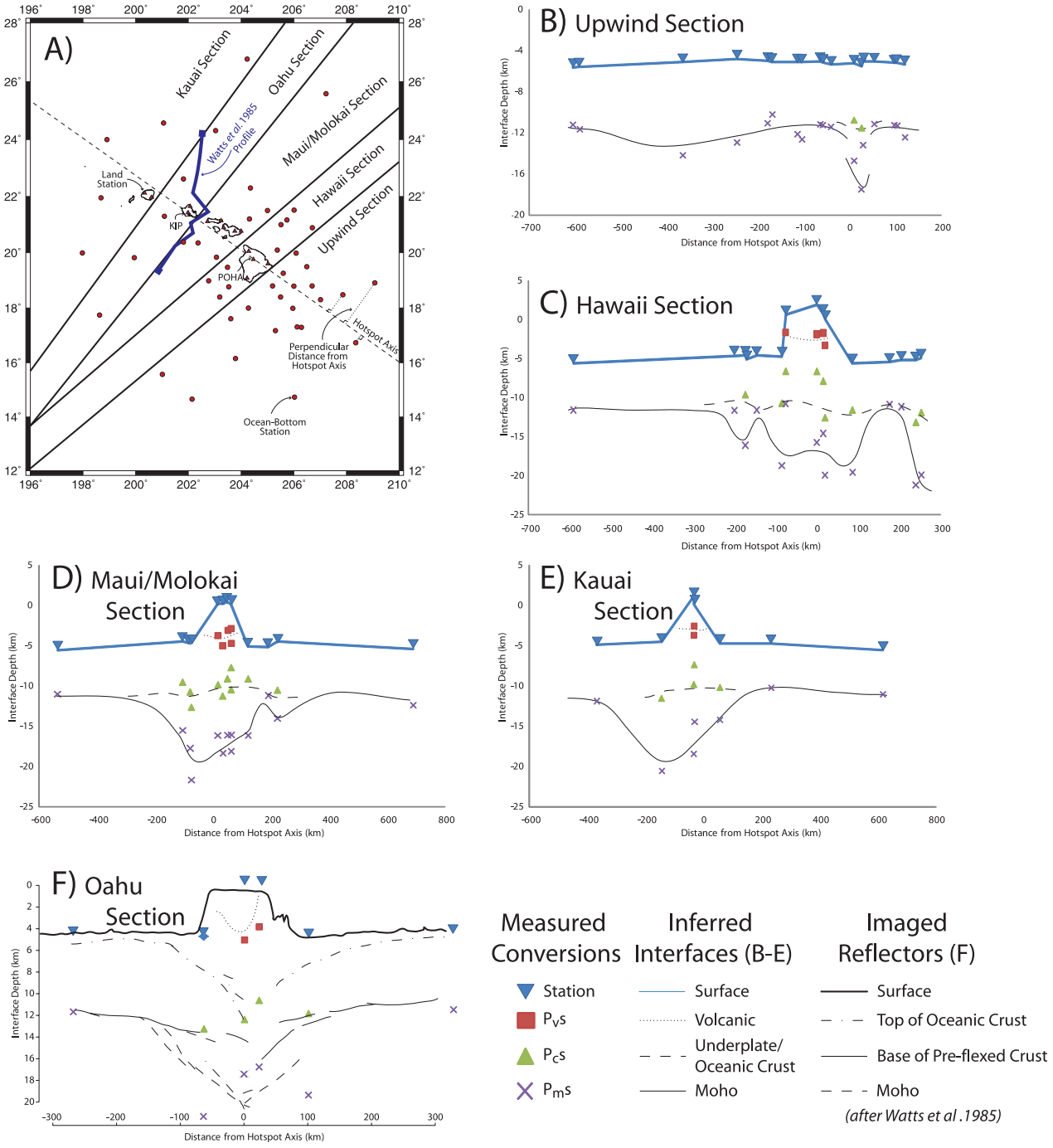

Figure 14. Cross-sections of the crust beneath the Hawaiian Swell. (a) Locations of sections. Stations (red circles) are grouped by section; for each section we plot the depth of *Ps* conversions at a given station as a function of horizontal distance to the hotspot axis (defined by a line connecting permanent stations POHA and KIP). The locations of the expanding spread profiles (ESPs) of Watts *et al.* (1985b) are shown as a blue line. In subsequent panels, station positions are indicated by blue triangles, $P_v s$ conversions as red squares, $P_c s$ conversions as green triangles, and $P_m s$ conversions as purple Xs. Schematic interfaces where present (blue line, surface; dotted line, base of volcanic material; dashed line, base of normal oceanic crust; solid line, Moho) are drawn to show possible structure. (b) Upwind section. Aside from a small finger of underplating approaching Hawaii (Fig. 12), crustal structure is relatively uniform. (c) Hawaii section. Underplating is indicated beneath the island and nearby stations. A break in underplating is visible at ±150 km from the centre of the island, outward of which underplating is again indicated. Although there is variability in the depth of the $P_c s$ conversion, it is tracked closely by the $P_v s$ conversion, maintaining an approximately constant thickness of the intervening layer. (d) Maui/Molokai section. Underplating is indicated beneath the island and nearby stations, with a notable break at +200 km. Mid-crustal interfaces are highly variable, but $P_v s$ and $P_c s$ correlate, maintaining an approximately constant thickness of the layer of normal oceanic crust (though it is notably thinner than the regional average, see Fig. 13). (e) Kauai section. Structure is largely similar to that in the Oahu section, with underplating present in the vicinity of the island. (f) Oahu section. We overlay our measurements of crustal interfaces on the structure derived by Watts *et al.* (1985b), obtained from ESPs along the path plotted in (a). Solid and dashed background lines represent prominent reflectors in their study. This section serves as a benchmark for the receiver function method and proposed average velocity model (Table 3) and indicates that the receiver function results compare favourably to those from the ESPs.

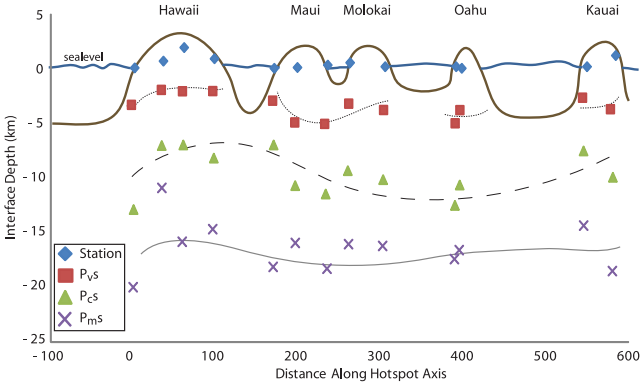

Figure 15. Depth to Moho along the Hawaiian Islands relative to sea level. See Fig. 14 for an explanation of other information. Our results indicate a relatively constant thickness of underplating along the island chain.

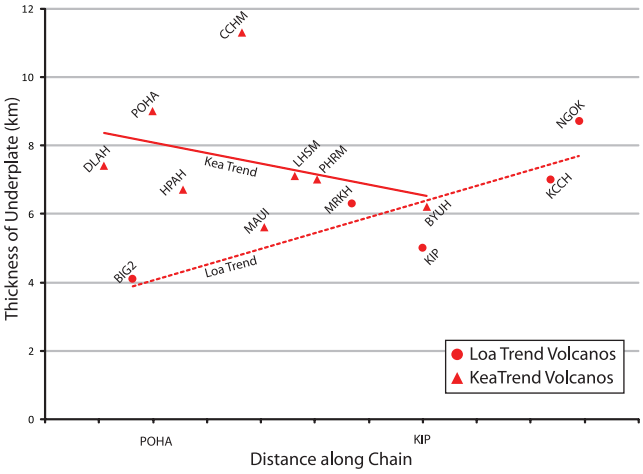

Figure 16. Thickness of underplated material along Kea and Loa volcanic trends. Identified Loa-trend stations (circles) and Kea-trend stations (triangles) appear to have anticorrelated underplating thicknesses. This difference vanishes at Oaku, as do the chemical trends.

This hypothesis is supported by the absence of underplating in the deepest portions of the Hawaiian moat (Fig. 12). While flexure due to volcanic loading of the plate certainly contributes to the bathymetric low, the deepest portion of the moat (due north of Hawaii) corresponds to a distinct and well-resolved region without imaged underplating. The bathymetric anomaly in this region is markedly deeper than other portions of the moat, and we propose that this difference is related to the deficit of underplated magma. The presence of a volume of comparatively high mantle seismic velocities that is parabola-shaped in map view (Wolfe *et al.* 2009), if a signature of anomalously low temperature and high density, may also contribute to the bathymetric anomaly.

To explore further the dependence of the swell bathymetry on crustal structure, we use an isostatic model (after Turcotte & Schubert 2002) to compute the average lithospheric thermal anomaly relative to a reference state. Flexure of the elastic lithosphere, of course, does play a large role in the response to chemical buoyancy, particularly for short-wavelength features such as the moat (Forsyth 1985). However, a simple model of periodic loading of a 25-km-thick elastic lithosphere suggests that the 500-km wavelength of the swell is approximately 50 per cent isostatically compensated (Turcotte & Schubert 2002). For simplicity in this calculation, we have not included land-based stations in this analysis, where topography clearly has substantial flexural support.

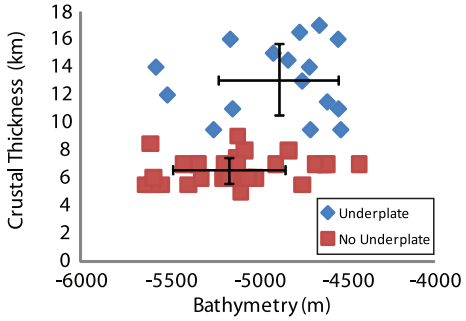

Figure 17. Depths of ocean-bottom stations compared to the crustal thicknesses obtained in this study. Blue diamonds are stations with underplating, and red squares are stations where no underplating is indicated. For each subset, averages and standard deviations (error bars) are calculated. Stations with notable underplating are on average shallower than stations with no underplating.

We assume that the vertically averaged lithospheric density $\overline{\rho_m}$ is a function of vertically averaged lithospheric thermal anomaly $\overline{\Delta T_m}$

$$\overline{\rho_m} = \rho_0(1 - \alpha\overline{\Delta T_m}), \tag{5}$$

where $\alpha = 10^{-5}$ is the volumetric coefficient of thermal expansion and ρ_0 is the vertically averaged lithospheric density in the absence of a thermal anomaly. For isostatic compensation at a depth $w =$ 150 km, we can derive a relation between observed bathymetry, crustal structure, and local mantle thermal anomaly. The reference state has bathymetry $z_0 = -5.2$ km and crustal thickness $c_0 =$ 6.5 km; the reference densities are $\rho_w = 1000\,\mathrm{kg\,m^{-3}}$ (water), $\rho_c = 2900\,\mathrm{kg\,m^{-3}}$ (crust), $\rho_w = 3100\,\mathrm{kg\,m^{-3}}$ (underplate) and $\rho_0 =$ $3300\,\mathrm{kg\,m^{-3}}$ (mantle). The local isostatic state is given by the local bathymetry z, crustal thickness c, and thickness u of underplated material. The pressure at the base of the reference column is

$$P_0 = (\rho_w - \rho_0)gz_0 + (\rho_c - \rho_0)gc_0 + \rho_0 gw, \tag{6}$$

where g is the gravitational acceleration, and the average lithospheric density at an observation point is

$$\overline{\rho_m} = \frac{P_0/g - z\rho_w - c\rho_c - u\rho_u}{w - z - c - u}. \tag{7}$$

We can use eqs (5)–(7) to predict the regional mantle thermal anomaly from the bathymetry measured at each OBS location. First, we consider a case where crustal thickness is uniformly 6.5 km, equivalent to the reference state (Fig. 18a). We additionally assume no underplating ($u = 0$). This calculation requires temperature to rise by 200–300 °C along the chain, similar in many respects to inferences from thermal rejuvenation models and anomalies in upper mantle seismic velocities seen in seismic tomography (Wolfe *et al.* 2009).

For comparison, we predict the regional mantle thermal anomaly using the crustal structure obtained in this study. Under these assumptions, the mantle temperature anomaly reduces markedly beneath the Hawaiian Swell and along the island chain (Fig. 18b). Most stations considered in this study lie within 50 °C of the reference mantle temperature. Given that lithospheric flexure damps the surface expression of sublithospheric thermal buoyancy, we anticipate that the absolute magnitudes of the thermal anomalies calculated here are underestimates, especially for small-wavelength features. However, because much of any thermal anomaly is placed below the

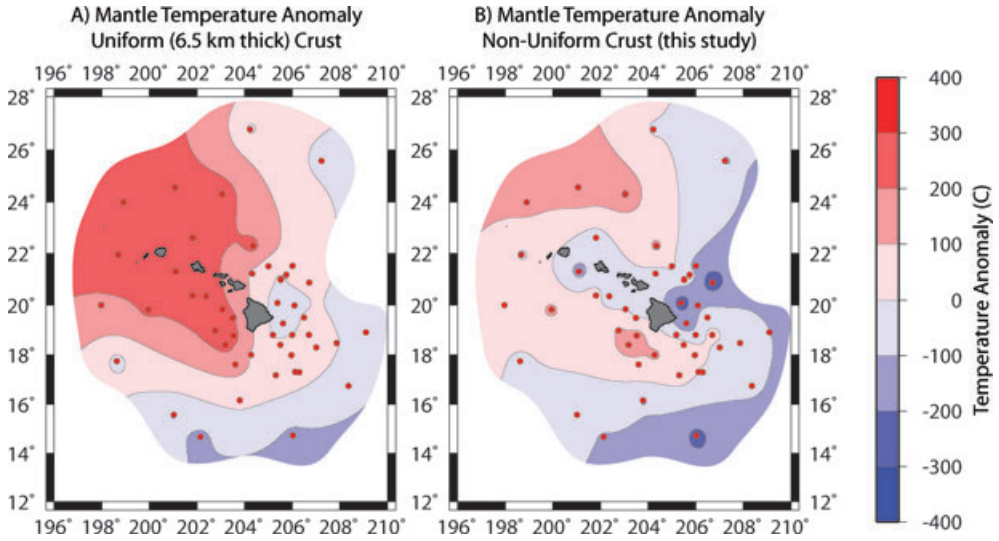

Figure 18. Average lithospheric thermal anomaly. (a) Thermal anomaly necessary to reproduce the Hawaiian Swell for a uniform crustal thickness of 6.5 km. (b) Thermal anomaly necessary to reproduce the Hawaiian Swell with the non-uniform crustal structure (local variability and underplating) obtained in this study. Contour intervals are 100 °C.

elastic lithosphere we expect both cases to be modified to a similar degree, preserving the contribution of crustal underplating.

This model is certainly an over-simplification. For example, we find that the amplitudes of the required thermal anomaly are sensitive to the depth of compensation. This is because, for a greater compensation depth, the buoyancy anomaly can be spread over a greater depth range, decreasing the thermal anomaly. Further, variations in mantle composition due to melt extraction at the base of the lithosphere will contribute buoyancy to the swell (e.g. Lodge & Helffrich 2006), reducing the magnitude of the thermal anomaly. These effects modify the amplitudes of our temperature fields but do not change the result that buoyancy from underplating contributes substantially to the bathymetric signal of the swell.

Although the presence of underplating adds buoyancy to the lithosphere that would otherwise be attributed to a mantle thermal anomaly, these results do not completely remove the need for a thermal anomaly in the mantle. The magnitude of the temperature anomaly required depends strongly on assumed material parameters and will likely adjust upwards with a more complete description of the problem. A more accurate determination of the mantle thermal anomaly will require a sophisticated analysis of lithospheric structure that is perhaps accessible with data collected by the Hawaiian PLUME seismic networks, but remains beyond the scope of this study. Further, a thermal anomaly deeper than the compensation depth will contribute only negligibly to the surface topography. Still, the presence of additional crustal buoyancy helps mitigate contradicting geophysical constraints. A large buoyancy anomaly is required by the bathymetry, but the small swell heat flow anomaly (Von Herzen *et al.* 1989) and low island subsidence rates at old ages (Phipps Morgan *et al.* 1995) suggest a small thermal anomaly.

As previously described, a notable feature of the bathymetry surrounding Hawaii is a deep and asymmetric moat, thought to result from volcanic loading. In both purely flexural and purely isostatic models, the lack of chemical buoyancy acts to increase the downward deflection of the seafloor. However, our results indicate that the swell arch may be partially supported by chemical buoyancy. Calculation of the thickness of the elastic lithosphere from the actual positions and depths of the moat and arch may therefore be overestimates. Watts & ten Brink (1989) show that underplating only beneath the volcanic load can decrease the elastic thickness by roughly a factor of two, but a lack of chemical support of the moat may decrease it further. By contrast, the moat near Oahu is underplated (Watts *et al.* 1985b) and is much shallower. The estimation of this parameter has important implications (as discussed above) for magma transport through the lithosphere, the initiation of volcanic islands, and subsequent melt focusing.

6 CONCLUSIONS

In this study, we analysed *P*-to-*s* converted phases to construct a regional model of crustal structure for the Hawaiian Swell. Our method permits the calculation of teleseismic receiver functions at sufficiently high frequencies to determine the thickness of the crust, either directly at high frequencies or indirectly at low frequencies, even using ocean-bottom instruments. Further, we have sufficient frequency resolution to determine whether an intracrustal conversion is present, signifying the presence of magmatic underplating. We find that the presence of underplating correlates with the shallow bathymetry of the Hawaiian Swell, suggesting that much of the swell is compositionally supported. This hypothesis reconciles the need for a buoyancy anomaly (previously thought to be thermal) in the mantle beneath the swell to fit the bathymetry with observations of normal seafloor heat flow in the area of the swell.

ACKNOWLEDGMENTS

We are grateful to the Ocean Sciences Division of the U.S. National Science Foundation for their support of this project under grants OCE-0002470, OCE-0002552 and OCE-0002819. We acknowledge the large number of individuals who contributed to the success of the PLUME project, particularly the contributions of R. Detrick and J. Orcutt, but also including the crews of the research vessels Melville, Ka'imikai-O-Kanaloa and Kilo Moana, the Jason remotely operated vehicle team, the Ocean Bottom Seismograph Instrument Pool, the SIO and WHOI OBS teams, the Carnegie Institution's portable seismology laboratory, and the hosts of temporary stations on the Hawaiian Islands. We thank R.S. White, an anonymous reviewer, E. Hauri, N. Shimizu, M. Kurz and others for

helpful comments on this manuscript. G. M. Leahy was supported by a Woods Hole Oceanographic Institution postdoctoral fellowship. Data from POHA, KIP, and MAUI were obtained from IRIS and are freely available to member institutions.

REFERENCES

Abouchami, W., Hofmann, A.W., Galer, S.J.G., Frey, F.A., Eisele, J. & Feigenson, M., 2005. Lead isotopes reveal bilateral asymmetry and vertical continuity in the Hawaiian mantle plume, *Nature,* **434,** 851–856.

Bianco, T.A., Ito, G., Becker, J.M. & Garcia, M.O., 2005. Secondary Hawaiian volcanism formed by flexural arch decompression, *Geochem. Geophys. Geosyst.,* **6,** Q08009, doi:10.1029/2005GC000945.

Brocher, T.M. & ten Brink, U.S., 1987. Variations in oceanic layer 2 elastic velocities near Hawaii and their correlation to lithospheric flexure, *J. geophys. Res.,* **92,** 2647–2661.

Caress, D., McNutt, M., Detrick, R. & Mutter, J., 1995. Seismic imaging of hotspot-related crustal underplating beneath the Marquesas Islands, *Nature,* **373,** 600–603.

Clague, D.A., 1987. Hawaiian alkaline volcanism, *Geol. Soc. Lond. Spec. Pub.,* **30,** 227–252.

Clague, D.A., Holcomb, R.T., Sinton, J.M., Detrick, R.S. & Torresan, M.E., 1990. Pliocene and Pleistocene alkalic flood basalts on the seafloor north of the Hawaiian Islands, *Earth planet. Sci. Lett.,* **98,** 175–191.

Constable, S. & Heinson, G., 2004. Hawaiian hot-spot swell structure from seafloor MT sounding, *Tectonophysics,* **389,** 111–124.

Crough, S.T., 1978. Thermal origin of mid-plate hot-spot swells, *Geophys. J. R. astr. Soc.,* **55,** 451–469.

Crough, S.T., 1983. Hotspot swells, *Ann. Rev. Earth Planet. Sci.,* **11,** 165–193.

Davies, G.F., 1992. Temporal variation of the Hawaiian plume flux, *Earth planet. Sci. Lett.,* **113,** 277–286.

DePaolo, D.J., Thomas, D.M., Stolper, E.M. & Garcia, M.O., 1999. Hawaii Scientific Drilling Project: Core Logs and Summarizing Data, rep, Calif. Inst. of Technol., Pasadena.

Detrick, R.S. & Crough, S.T., 1978. Island subsidence, hot spots, and lithospheric thinning, *J. geophys. Res.,* **83,** 1236–1244.

Dietz, R.S. & Menard, H.W., 1953. Hawaiian Swell, deep, and arch, and subsidence of the Hawaiian Islands, *J. Geol.,* **61,** 99–113.

Duncan, R.A. & Keller, R.A., 2004. Radiometric ages for basement rocks from the Emperor Seamounts, ODP Leg 197, *Geochem. Geophys. Geosyst.,* **5,** Q08L03, doi:10.1029/2004GC000704.

Eccles, J.D., White, R.S. & Christie, P.A.F., 2009. Identification and inversion of converted shear waves: case studies from the European North Atlantic continental margins, *Geophys. J. Int,* **179,** 381–400.

Forsyth, D.W., 1985. Subsurface loading and estimates of the flexural rigidity of continental lithosphere, *J. geophys. Res.,* **90,** 12 623–12 632.

Griggs, R.W., 1997. Paleoceanography of coral reefs in the Hawaiian-Emperor Chain–revisited, *Coral Reefs,* **16**(Suppl.), S33–S38.

Harland, K.E., White, R.S. & Soosalu, H., 2009. Crustal structure beneath the Faroe Islands from teleseismic receiver functions, *Geophys. J. Int.,* **177,** 115–124.

Harris, R.N. & McNutt, M.K., 2007. Heat flow on hot spot swells: evidence for fluid flow, *J. geophys. Res.,* **112,** B03407, doi:10.1029/2006JB004299.

Harris, R.N., Von Herzen, R.P., McNutt, M.K., Garven, G. & Jordahl, K., 2000. Submarine hydrogeology of the Hawaiian archipelagic apron 1. Heat flow patterns north of Oahu and Maro Reef, *J. geophys. Res.,* **105,** 21 353–21 369.

Hart, S.R., Hauri, E.H., Oschmann, L.A. & Whitehead, J.A., 1992. Mantle plumes and entrainment: isotopic evidence, *Science,* **256,** 517–520.

Hieronymus, C. & Bercovici, D., 1999. Discrete alternating hotspot islands formed by interaction of magma transport and lithospheric flexure, *Nature,* **397,** 604–607.

Hieronymus, C. & Bercovici, D., 2000. Non-hotspot formation of volcanic chains: control of tectonic and flexural stresses on magma transport, *Earth planet. Sci. Lett.,* **181,** 539–554.

Hieronymus, C. & Bercovici, D., 2001. A theoretical model of hotspot volcanism: control on volcanic spacing and patterns via magma dynamics and lithospheric stresses, *J. geophys. Res.,* **106,** 683–702.

Hofmann, A., 1997. Mantle geochemistry: the message from oceanic volcanism, *Nature,* **385,** 219–228.

Holbrook, W.S. & Kelemen, P.B., 1993. Large igneous province on the US Atlantic margin and implications for magmatism during continental breakup, *Nature,* **364,** 433–436.

Ihinger, P.D., 1995. Mantle flow beneath the Pacific plate: evidence from seamount segments in the Hawaiian-Emperor chain, *Am. J. Sci.,* **295,** 1035–1057.

Kelemen, P.B., Hirth, G., Shimizu, N., Spiegelman, M. & Dick, H.J.B., 1997. A review of melt migration processes in the adiabatically upwelling mantle beneath oceanic spreading ridges, *Phil. Trans. R. Soc. Lond. A,* **355,** 283–318.

Korenaga, J. & Kelemen, P.B., 1997. Origin of gabbro sills in the Moho transition zone of the Oman ophiolite: implications for magma transport in the oceanic lower crust, *J. geophys. Res.,* **102,** 27 729–27 749.

Laske, G., Phipps Morgan, J. & Orcutt, J.A., 1999. First results from the Hawaiian SWELL pilot experiment, *Geophys. Res. Lett.,* **26,** 3397–3400.

Laske, G., Phipps Morgan, J. & Orcutt, J.A., 2007. The Hawaiian SWELL pilot experiment—evidence for lithosphere rejuvenation from ocean bottom surface wave data, in *Plates, Plumes, and Planetary Processes,* Special Paper 430, pp. 209–233, eds Foulger, G.R. & Jurdy, D.M., Geological Society of America, Boulder, CO.

Laske, G., Collins, J.A., Wolfe, C.J., Solomon, S.C., Detrick, R.S., Orcutt, J.A., Bercovici, D. & Hauri, E.H., 2009. Probing the Hawaiian hot spot with new broadband ocean bottom instruments, *EOS, Trans. Am. geophys. Un.,* **90,** 362–363.

Leahy, G.M. & Collins, J.A., 2009. Improved statistical processing for common conversion point stacked receiver functions, *Bull. seism. Soc. Am.,* **99,** 914–921.

Leahy, G.M. & Park, J., 2005. Hunting for oceanic island Moho., *Geophys. J. Int.,* **160,** 1020–1026.

Li, X., Kind, R., Yuan, X., Wölbern, I. & Hanka, W., 2004. Rejuvenation of the lithosphere by the Hawaiian plume, *Nature,* **427,** 827–829.

Li, Y.P., Thurber, C.H. & Munson, C.G., 1992. Profile of discontinuities beneath Hawaii from S to P converted seismic-waves, *Geophys. Res. Lett.,* **19,** 111–114.

Lindwall, D.A., 1988. A two-dimensional seismic investigation of crustal structure under the Hawaiian Islands near Oahu and Kauai, *J. geophys. Res.,* **93,** 12 107–12 122.

Lindwall, D.A., 1991. Old Pacific crust near Hawaii—a seismic view, *J. geophys. Res.,* **96,** 8191–8203.

Lister, J.R. & Kerr, R.C., 1991. Fluid-mechanical models of crack propagation and their application to magma transport in dykes, *J. geophys. Res.,* **96,** 10 049–10 077.

Lodge, A. & Helffrich, G., 2006. Depleted swell root beneath the Cape Verde Islands, *Geology,* **34,** 449–452.

McKenzie, D., 1984. The generation and compaction of partially molten rock, *J. Petrol.,* **25**(Part 3), 713–765.

McNutt, M. & Bonneville, A., 2000. A shallow, chemical origin for the Marquesas Swell, *Geochem. Geophys. Geosyst.,* **1,** 1014, doi:10.1029/1999GC000028.

Montelli, R., Nolet, G., Dahlen, F.A., Masters, G., Engdahl, E.R. & Hung, S.H., 2004. Finite-frequency tomography reveals a variety of plumes in the mantle, *Science,* **303,** 338–343.

Montelli, R., Nolet, G., Dahlen, F.A. & Masters, G., 2006. A catalogue of deep mantle plumes: new results from finite-frequency tomography, *Geochem. Geophys. Geosyst.,* **7,** Q11007, doi:10.1029/2006GC001248.

Moore, W.B., Schubert, G. & Tackley, P., 1998. Three-dimensional simulations of plume-lithosphere interaction at the Hawaiian swell, *Science,* **279,** 1008–1011.

Morgan, J.W., 1971. Convection plumes in the lower mantle, *Nature,* **230,** 42–43.

Muller, J.R., Ito, G. & Martel, S.J., 2001. Effects of volcano loading on dike propagation in an elastic half-space, *J. geophys. Res.,* **106,** 11 101–11 113.

Müller, R.D., Sdrolias, M., Gaina, C. & Roest, W.R., 2008. Age, spreading rates and spreading symmetry of the world's ocean crust, *Geochem. Geophys. Geosyst.,* **9,** Q04006, doi:10.1029/2007GC001743.

National Geophysical Data Center, 2006. 2-minute Gridded Global Relief Data (ETOPO2v2), http://www.ngdc.noaa.gov/mgg/fliers/06mgg01.html, National Oceanic and Atmospheric Administration, U.S. Department of Commerce.

Park, J. & Levin, V., 2000. Receiver functions from multiple-taper spectral correlation estimates, *Bull. seism. Soc. Am.,* **90,** 1507–1520.

Park, J. & Levin, V., 2010. Receiver functions from multiple-taper spectral correlation: statistics, single-station migration, and jackknife uncertainty, *Geophys. J. Int,* submitted.

Park, J., Morgan, J.K., Zelt, C.A., Okubo, P.G., Peters, L. & Benesh, N., 2007. Comparative velocity structure of active Hawaiian volcanoes from 3-D onshore-offshore seismic tomography, *Earth planet. Sci. Lett.,* **259,** 500–516.

Parsons, B. & Sclater, J.G., 1977. An analysis of the variation of ocean floor bathymetry and heat flow with age, *J. geophys. Res.,* **82,** 802–827.

Phipps Morgan, J., Morgan, W.J. & Price, E., 1995. Hotspot melting generates both hotspot volcanism and a hotspot swell, *J. geophys. Res.,* **100,** 8045–8062.

Priestley, K. & Tilmann, F., 1999. Shear-wave structure of the lithosphere above the Hawaiian hot spot from two-station Rayleigh wave phase velocity measurements, *Geophys. Res. Lett.,* **26,** 1493–1496.

Ribe, N.M. & Christensen, U.R., 1994. Three-dimensional modeling of plume-lithosphere interaction, *J. geophys. Res.,* **99,** 669–682.

Robinson, E.M., 1988. The topographic and gravitational expression of density anomalies due to melt extraction in the uppermost oceanic mantle, *Earth planet. Sci. Lett.,* **90,** 221–228.

Rubin, A.M., 1995. Propagation of magma-filled cracks, *Ann. Rev. Earth planet. Sci.,* **23,** 287–336.

Schubert, G., Turcotte, D. & Olson, P., 2001. *Mantle Convection in the Earth and Planets,* Cambridge Univ. Press, New York.

Sleep, N.H., 1987. Lithospheric heating by mantle plumes, *Geophys. J. R. astr. Soc.,* **91,** 1–11.

Sleep, N.H., 1990. Hotspots and mantle plumes—some phenomenology, *J. geophys. Res.,* **95,** 6715–6736.

Sleep, N.H., 1992. Hotspot volcanism and mantle plumes, *Ann. Rev. Earth planet. Sci.,* **20,** 19–43.

Sleep, N.H., 1994. Lithospheric thinning by midplate mantle plumes and the thermal history of hot plume material ponded at sublithospheric depths, *J. geophys. Res.,* **99,** 9327–9343.

Sparks, D.W. & Parmentier, E.M., 1991. Melt extraction from the mantle beneath spreading centers, *Earth planet. Sci. Lett.,* **105,** 368–377.

Spiegelman, M., 1993. Physics of melt extraction: theory, implications and applications, *Phil. Trans. R. Soc. Lond., A,* **342,** 23–41.

Stein, C.A. & Stein, S., 1992. A model for the global variation in oceanic depth and heat flow with lithospheric ages, *Nature,* **359,** 123–129.

ten Brink, U.S., 1991. Volcano spacing and plate rigidity, *Geology,* **19,** 397–400.

ten Brink, U.S. & Brocher, T.M., 1987. Multichannel seismic evidence for A subcrustal intrusive complex under Oahu and a model for Hawaiian volcanism, *J. geophys. Res.,* **92,** 13 687–13 707.

ten Brink, U.S. & Brocher, T.M., 1988. Multichannel seismic evidence for fariations in crustal thickness across the Molokai Fracture Zone in the mid-Pacific, *J. geophys. Res.,* **93,** 1119–1130.

Tilmann, F., Benz, H., Priestley, K. & Okubo, P., 2001. P-wave velocity structure of the uppermost mantle beneath Hawaii from traveltime tomography, *Geophys. J. Int.,* **146,** 594–606.

Turcotte, D. & Schubert, G., 2002. *Geodynamics,* 2nd edn, Cambridge Univ. Press, New York.

Van Ark, E. & Lin, J., 2004. Time variation in igneous volume flux of the Hawaii-Emperor hot spot seamount chain, *J. geophys. Res.,* **109,** B11401, doi:10.1029/2003JB002949.

Verzhbitsky, E.V., Kononov, M.V., Byakov, A.F. & Dulub, V.P., 2006. Evolution of the lithosphere of the Hawaiian-Emperor seamount chain, Pacific Ocean, as inferred from geophysical data, *Geotectonics,* **40,** 467–480.

Vidal, V. & Bonneville, A., 2004. Variations of the Hawaiian hot spot activity revealed by variations in the magma production rate, *J. geophys. Res.,* **109,** B03104, doi:10.1029/2003JB00259.

Von Herzen, R.P., Cordery, M.J., Detrick, R.S. & Fang, C., 1989. Heat flow and the thermal origin of hot spot swells—the Hawaiian Swell revisited, *J. geophys. Res.,* **94,** 13 783–13 799.

Watts, A.B. & ten Brink, U.S., 1989. Crustal structure, flexure, and subsidence history of the Hawaiian Islands, *J. geophys. Res.,* **94,** 10 473–10 500.

Watts, A.B., McKenzie, D.P., Parsons, B.E. & Roufosse, M., 1985a. The relationship between gravity and bathymetry in the Pacific Ocean, *Geophys. J. R. astr. Soc.,* **83,** 263–298.

Watts, A.B., ten Brink, U.S., Buhl, P. & Brocher, T.M., 1985b. A multichannel seismic study of lithospheric flexure across the Hawaiian-Emperor seamount chain, *Nature,* **315,** 105–111.

Wessel, P., 1993a. A reexamination of the flexural deformation beneath the Hawaiian Islands, *J. geophys. Res.,* **98,** 12 177–12 190.

Wessel, P., 1993b. Observational constraints on models of the Hawaiian hotspot swell, *J. geophys. Res.,* **98,** 16 095–16 104.

White, R.S. & McKenzie, D., 1995. Mantle plumes and flood basalts, *J. geophys. Res.,* **100,** 17 543–17 585.

White, R.S. & Smith, L.K., 2009. Crustal structure of the Hatton and the conjugate east Greenland rifted volcanic continental margins, NE Atlantic, *J. geophys. Res.,* **114,** B02305, doi:10.1029/2008JB005856.

Wölbern, I., Jacob, A.W.B., Blake, T.A., Kind, R., Li, X., Yuan, X., Duennebier, F. & Weber, M., 2006. Deep origin of the Hawaiian tilted plume conduit derived from receiver functions, *Geophys. J. Int.,* **166,** 767–781.

Wolfe, C.J., NcNutt, M.K. & Detrick, R.S., 1994. The Marquesas archipelagic apron: seismic stratigraphy and implications for volcano growth, mass wasting, and crustal underplating, *J. geophys. Res.,* **99**(B7), 13 591–13 608.

Wolfe, C.J., Solomon, S.C., Silver, P.G., vanDecar, J.C. & Russo, R.M., 2002. Inversion of body-wave delay times for mantle structure beneath the Hawaiian Islands: results from the PELENET experiment, *Earth planet. Sci. Lett,* **198,** 129–145.

Wolfe, C.J., Solomon, S.C., Laske, G., Collins, J.A., Detrick, R.S., Orcutt, J.A., Bercovici, D. & Hauri, E., 2009. Mantle shear-wave velocity structure beneath the Hawaiian hotspot, *Science,* **326,** 1388–1390.

Woods, M.T. & Okal, E.A., 1996. Rayleigh-wave dispersion along the Hawaiian Swell: a test of lithospheric thinning by thermal rejuvenation at a hotspot, *Geophys. J. Int.,* **125,** 325–339.

Woods, M.T., Leveque, J.J., Okal, E.A. & Cara, M., 1991. Two-station measurements of Rayleigh wave group velocity along the Hawai'ian Swell, *Geophys. Res. Lett.,* **18,** 105–108.

Zhong, S.J., Ritzwoller, M., Shapiro, N., Landuyt, W., Huang, J.S. & Wessel, P., 2007. Bathymetry of the Pacific plate and its implications for thermal evolution of lithosphere and mantle dynamics, *J. geophys. Res.,* **112,** B06412, doi:10.1029/2006JB004628.

Zhu, L. & Kanamori, H., 2000. Moho depth variation in southern California from teleseismic receiver functions, *J. geophys. Res.,* **105,** 2969–2980.

SUPPORTING INFORMATION

Additional Supporting Information may be found in the online version of this article:

Figure S1. Map of PLUME stations and the bathymetry of the Hawaiian Swell.
Figure S2. Receiver functions from land stations.
Figure S3. Receiver functions for ocean-bottom stations.

Please note: Wiley-Blackwell are not responsible for the content or functionality of any supporting materials supplied by the authors. Any queries (other than missing material) should be directed to the corresponding author for the article.